Statistical Shape Analysis using Topological Data Analysis

Part III: Real Applications

Chul Moon

Southern Methodist University
chulm@smu.edu
https://github.com/chulmoon/TDA-lecture

ECSSC 2021
25 July 2021

Outline

Outline

Application to Fingerprint Classification

Do we need better methods for fingerprints?

- Three types of fingerprints by Galton (1892)

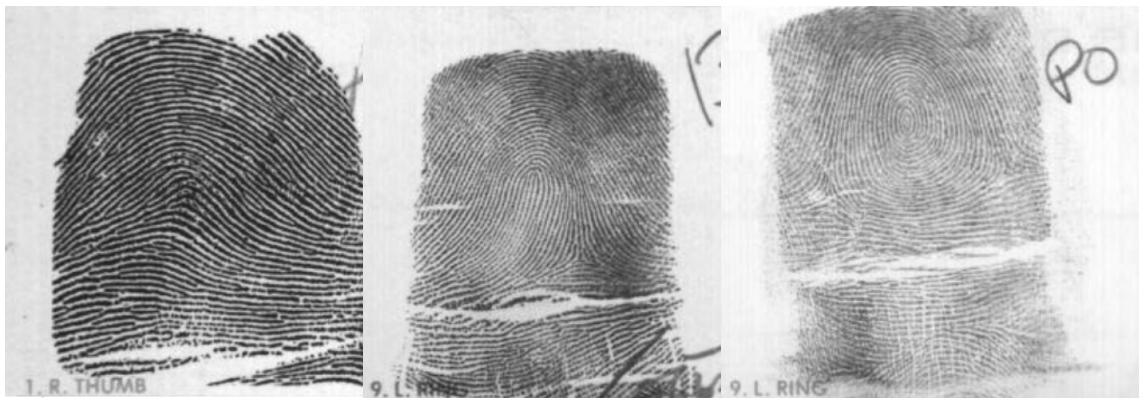

(a) arch (b) loop (c) whorl

- Research objective: classify fingerprints into three classes – arch, loop and whorl – using topological data analysis

Minutiae: Major Features of Fingerprints

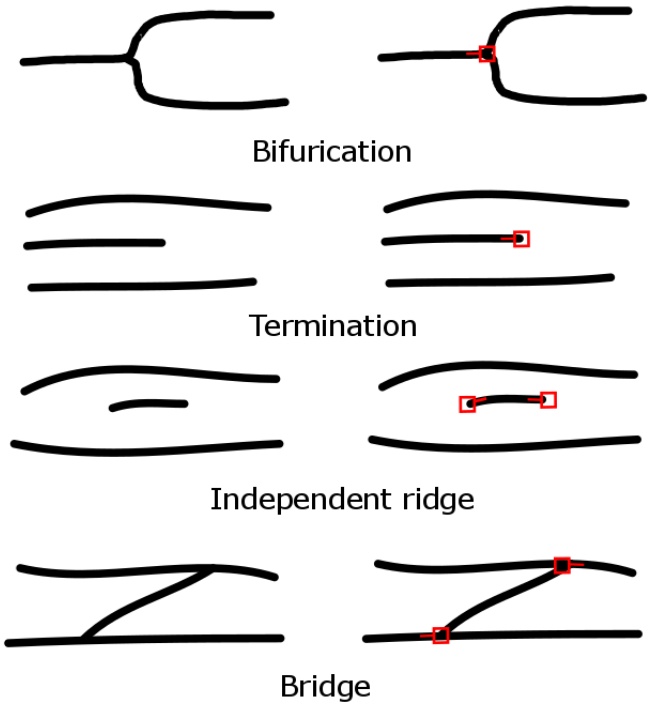

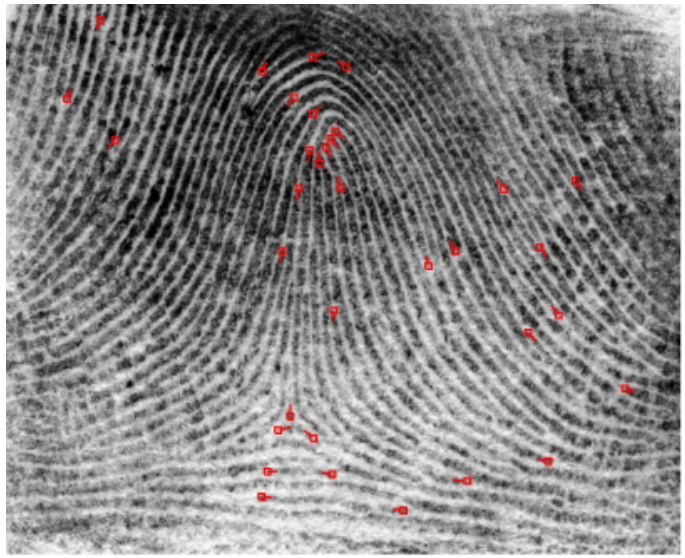

- Minutiae are specific patterns in a fingerprint
- Minutia point p_i includes location and orientation $p_i = (x_i, y_i, \theta_i) \in \mathbb{R}^2 \times S^1$

Defining a Metric Space for Minutiae Points

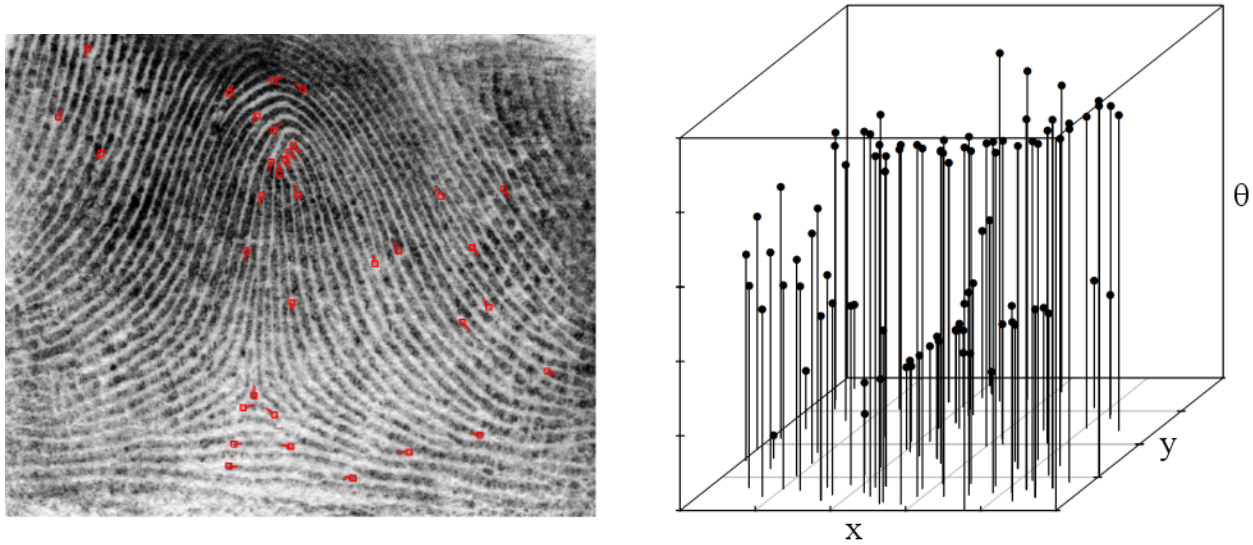

Figure: Minutiae points on $\mathbb{R}^2 \times S^1$ space

- Define a metric space considering both location and orientation

$$d(p_i, p_j) = \lambda * \left(\frac{1}{\sqrt{2}} \sqrt{(x_i - x_j)^2 + (y_i - y_j)^2} \right) + (1 - \lambda)\theta_{ij},$$

$$\text{where } \theta_{ij} = \frac{1}{2\pi} |\theta_i - \theta_j|$$

- Compute persistent homology for the metric space

Persistent Homology Computation Result

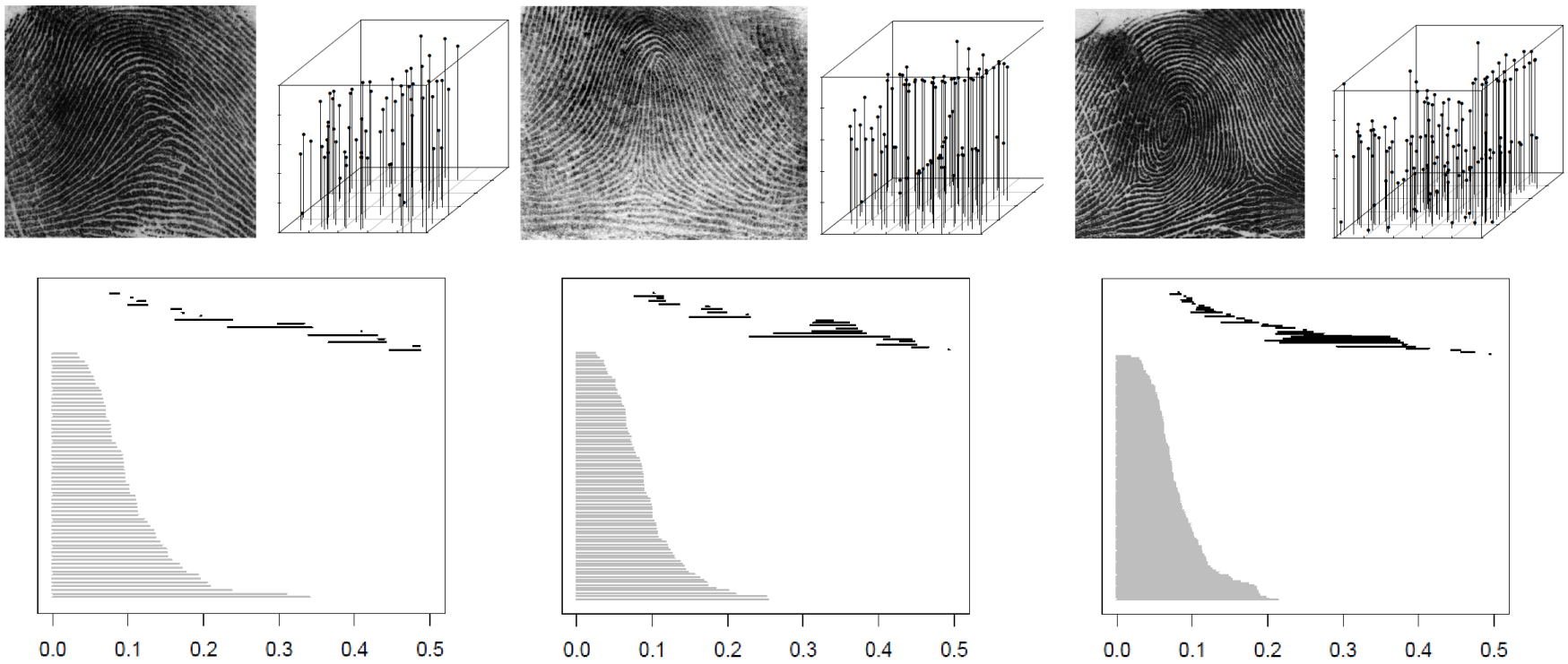

(a) arch (b) loop (c) whorl

Feature Extraction: Intervals to Vector

- To be used in classification algorithms, multisets of intervals need to be converted into vector format
- Suggest features for interval [Birth, Death]

Compute features:

1. Statistical features
2. Polynomial features
3. Regression coefficients

$\Longrightarrow$ We obtain 552 features for one fingerprint image

Fingerprint Classification Result

Results

- NIST database SD-27 including 258 fingerprints
- Feature selection using correlation and backward elimination
- Train a linear discriminant analysis (LDA) classifier using the leave-one-out-cross-validation (LOOCV)
- Highest classification rate is 93.1% (32 features used)

Conclusion

- Achieve near state-of-the-art classification accuracy rates by using minimum pre-processing processes and a stricter success rule
- The first paper that applies topological data analysis to fingerprint data

Finding Cosmic Void and Filament Loops

- Cosmic void and loops of filaments in universe
- Dark matter halo investigation

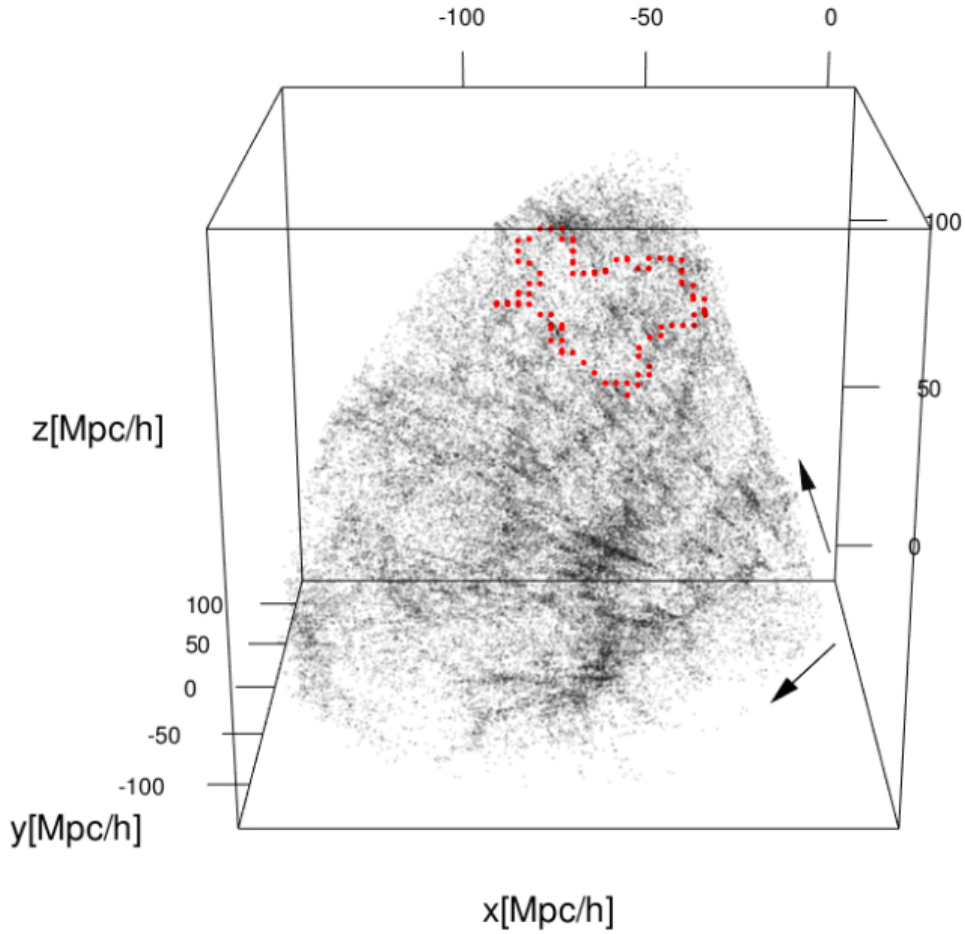

Figure: Figure from Xu et al. (2019)

Identify Locations and Generators via TDA

- Xu et al. (2019) propose to use TDA to identify locations of cosmic void and filament loops and generators

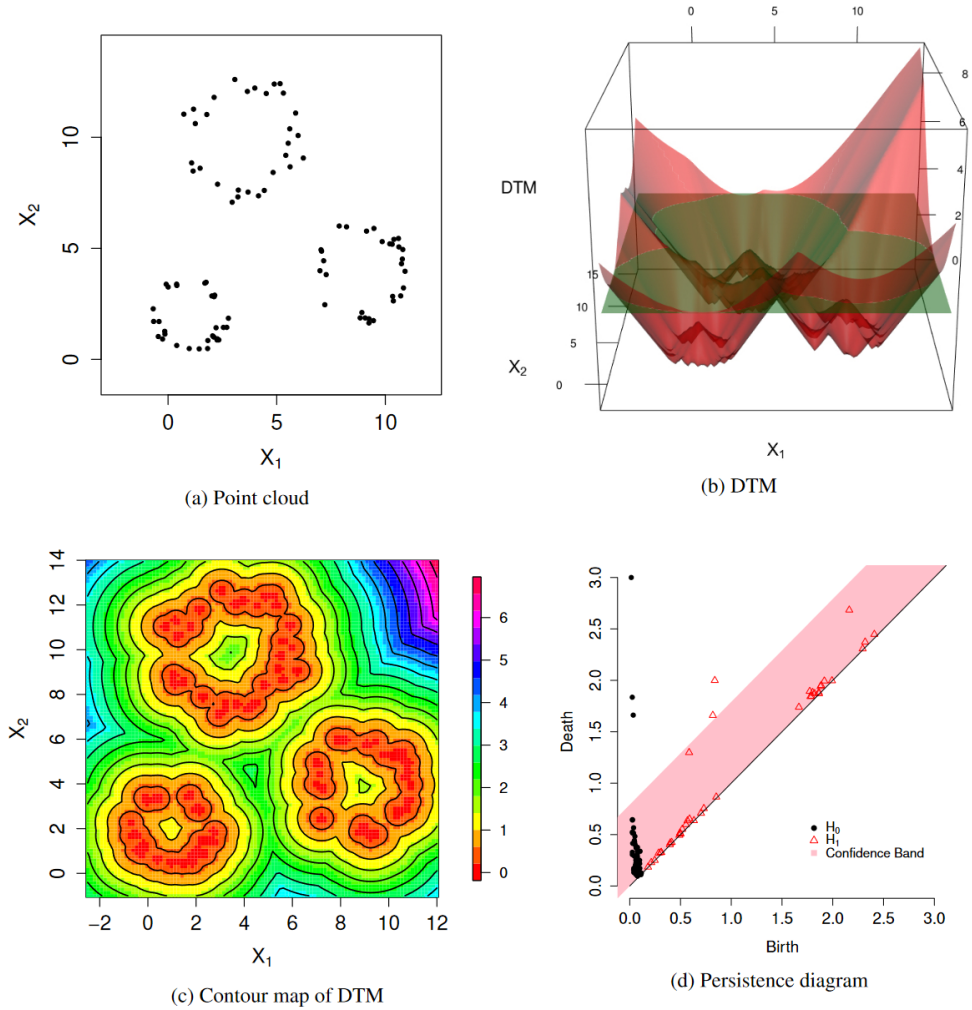

Figure: Figure from Xu et al. (2019)

Application to Galaxy Data

- Xu et al. (2019) locate statistically significant voids, and voids

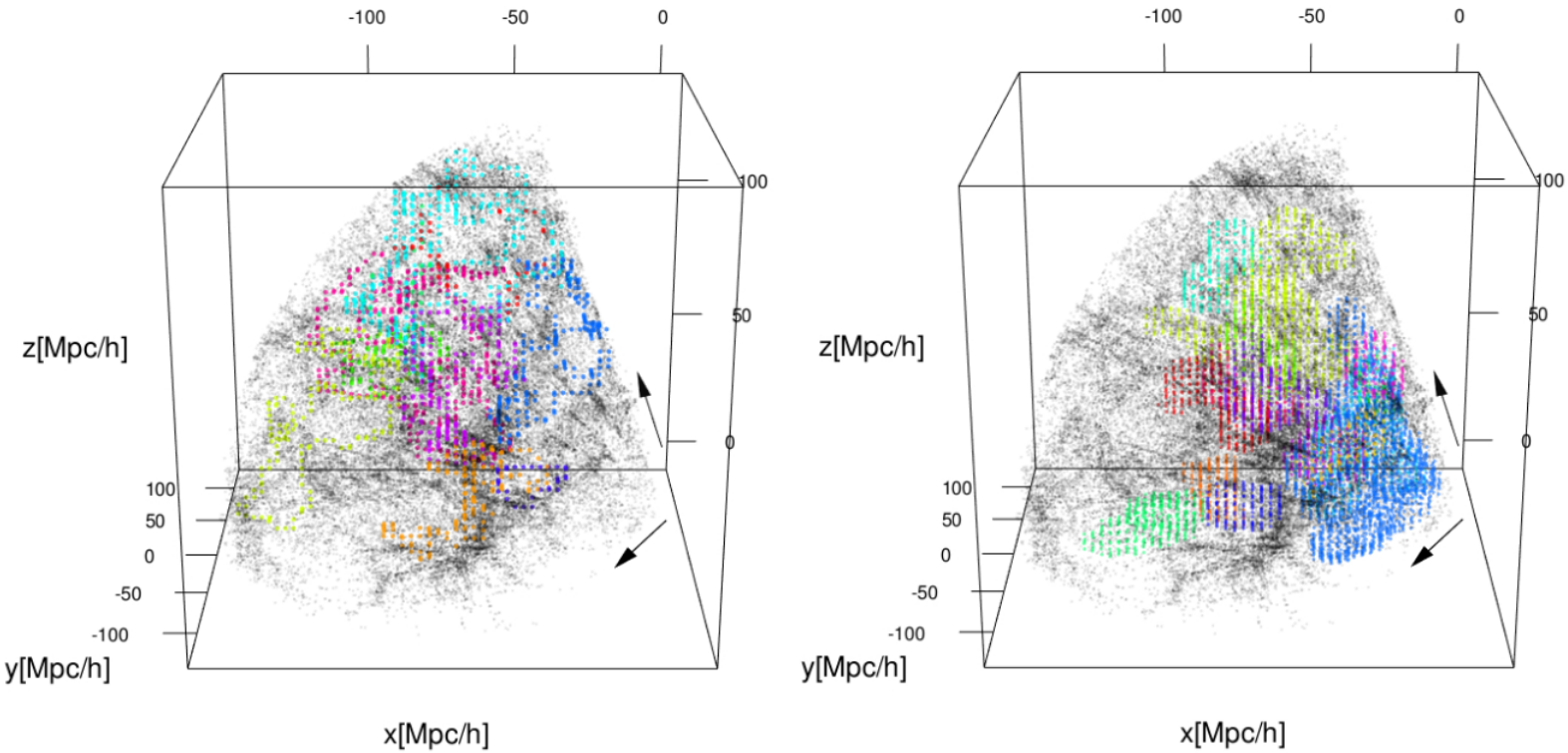

(a) Filament loops, H_1

(b) Cosmic voids, H_2

Figure: Figure from Xu et al. (2019)

Outline

Study of Rocks Using Rock Image Data

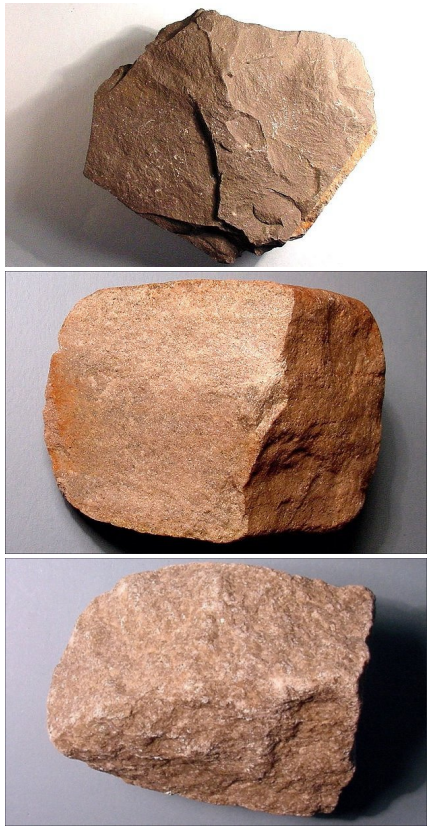

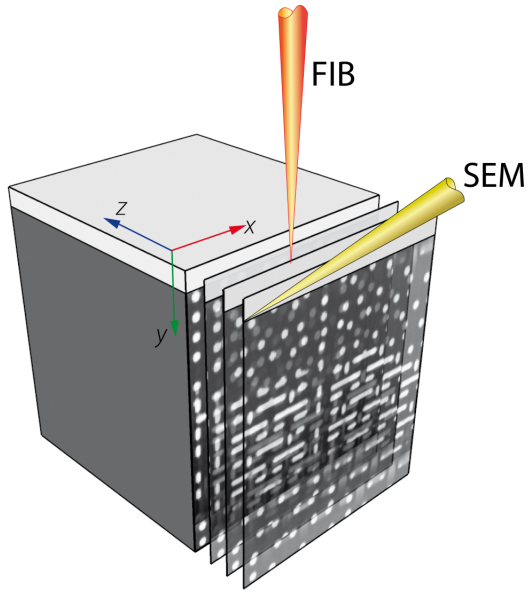

Figure: Figures from Stelma (2004); Weller (2004); Davami (2015)

Data of Interest: Binarized Material Images

- Original scanned images are grayscale images
- We only consider binary images in this presentation; applications are not limited to binary images

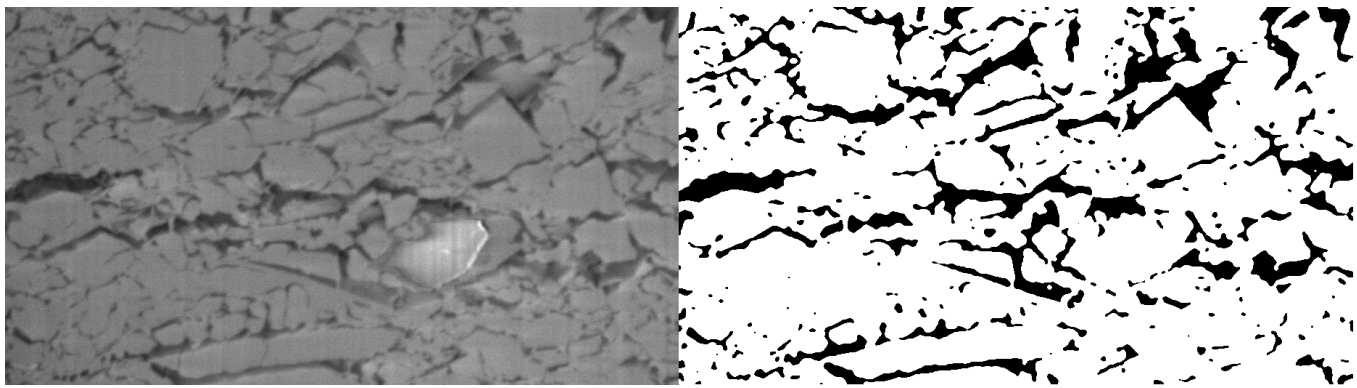

Figure: Original grayscale image and binarized image of Selma Chalk

Traditional Approaches on Rock Physics

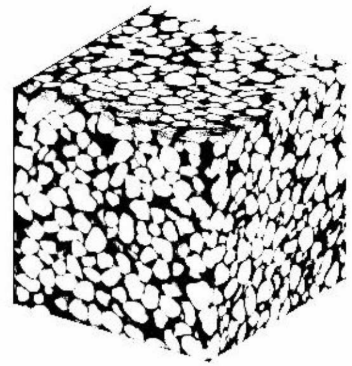

$\longrightarrow$ *Porosity*
Permeability
Anisotropy
...

Figure: Figure from Talabi et al. (2009)

Rock image data – (Simulations) → Estimate geophysical properties

- Models include limiting geometrical assumptions
- High computational cost

Topological data analysis provides numerical summary of structure and connectivity of rocks

Homology of Rock Image Data?

- 2-phase binary image $\rightarrow$ Multiscale image
- Robins et al. (2016) derive geometric characteristics from binary image using the Signed Euclidean Distance Transform (SEDT)
- Grain – Positive vs. Pore – Negative
- Euclidean distance to the opposite phase

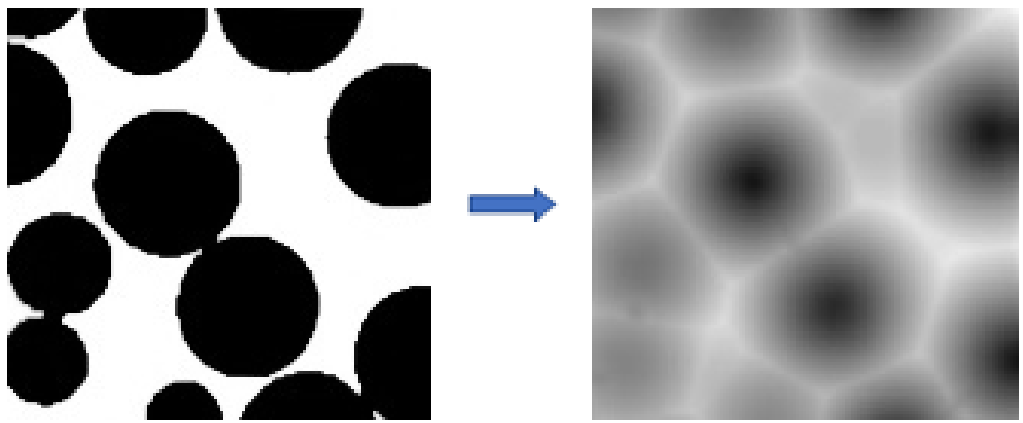

Constructing Complex

- Multiscale image $\rightarrow$ Complex
- Set the level-set filtration on SEDT value
- Start in the pore phase (negative), moving up to the grain phase (positive)

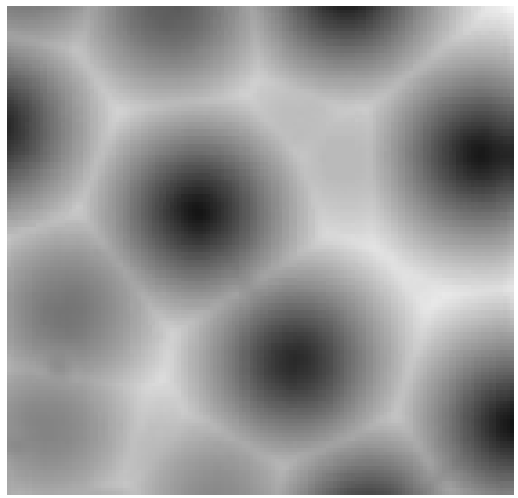

Constructing Complex

- Multiscale image $\rightarrow$ Complex
- Set the level-set filtration on SEDT value
- Start in the pore phase (negative), moving up to the grain phase (positive)

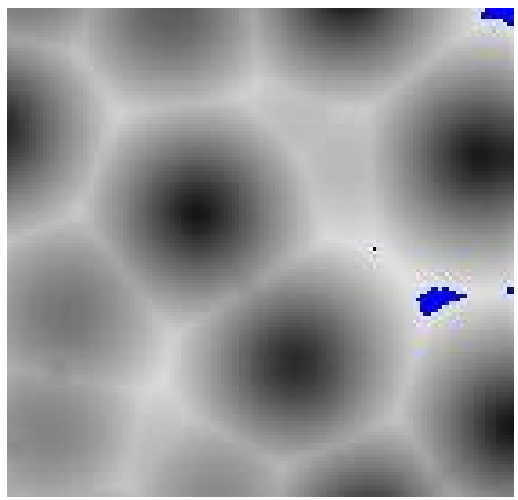

Constructing Complex

- Multiscale image $\rightarrow$ Complex
- Set the level-set filtration on SEDT value
- Start in the pore phase (negative), moving up to the grain phase (positive)

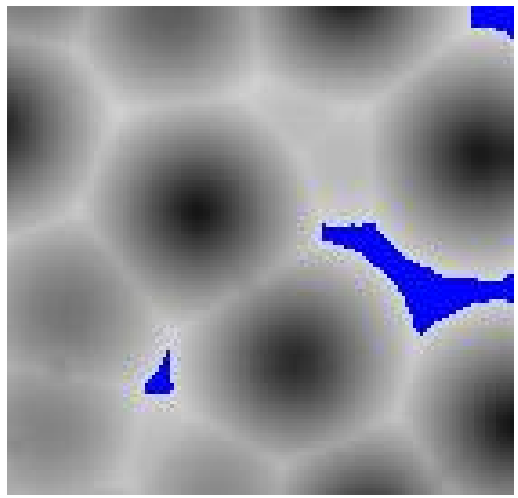

Constructing Complex

- Multiscale image $\rightarrow$ Complex
- Set the level-set filtration on SEDT value
- Start in the pore phase (negative), moving up to the grain phase (positive)

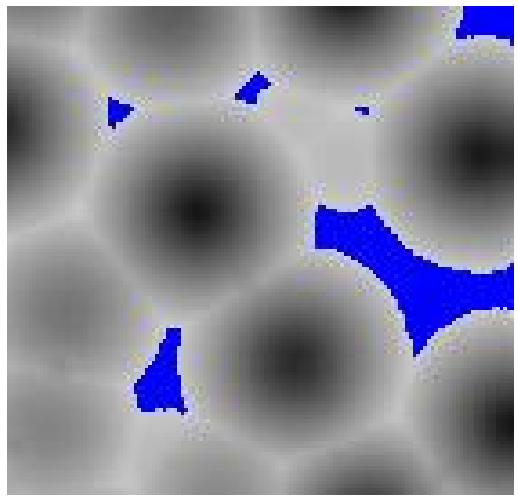

Constructing Complex

- Multiscale image $\rightarrow$ Complex
- Set the level-set filtration on SEDT value
- Start in the pore phase (negative), moving up to the grain phase (positive)

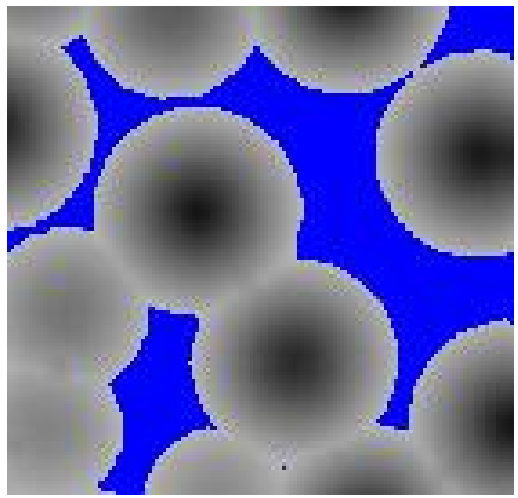

Constructing Complex

- Multiscale image $\rightarrow$ Complex
- Set the level-set filtration on SEDT value
- Start in the pore phase (negative), moving up to the grain phase (positive)

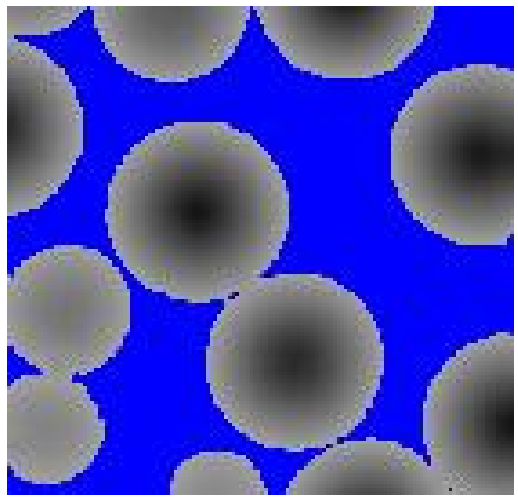

Constructing Complex

- Multiscale image $\rightarrow$ Complex
- Set the level-set filtration on SEDT value
- Start in the pore phase (negative), moving up to the grain phase (positive)

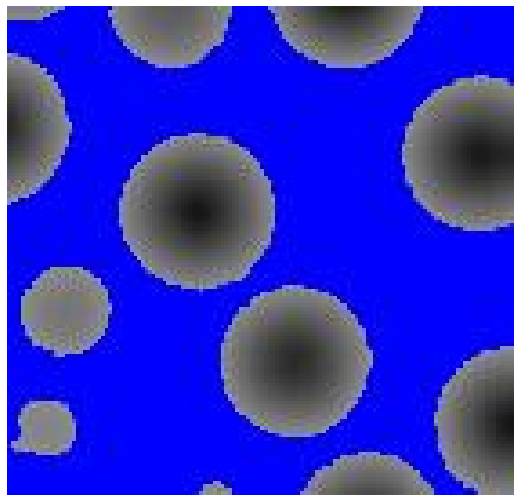

Constructing Complex

- Multiscale image $\rightarrow$ Complex
- Set the level-set filtration on SEDT value
- Start in the pore phase (negative), moving up to the grain phase (positive)

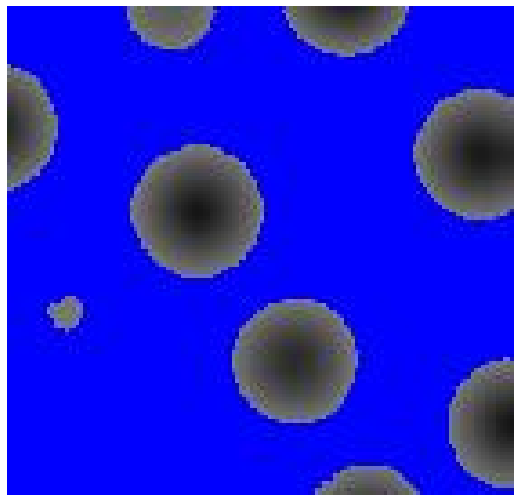

Constructing Complex

- Multiscale image $\rightarrow$ Complex
- Set the level-set filtration on SEDT value
- Start in the pore phase (negative), moving up to the grain phase (positive)

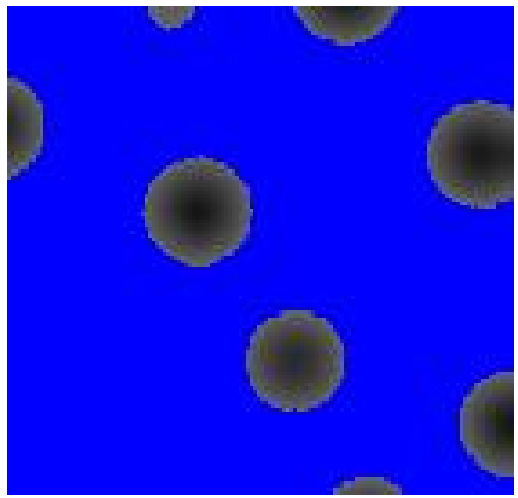

Constructing Complex

- Multiscale image $\rightarrow$ Complex
- Set the level-set filtration on SEDT value
- Start in the pore phase (negative), moving up to the grain phase (positive)

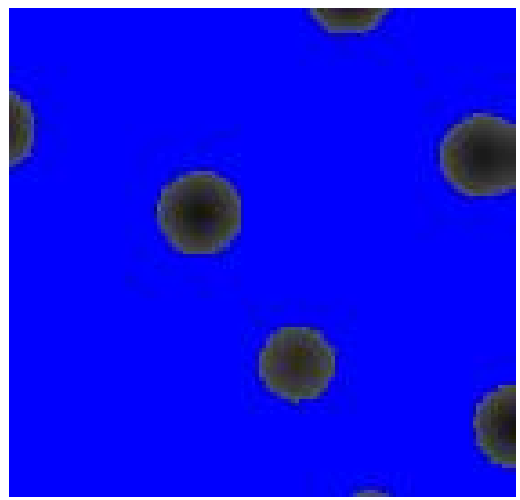

Topological Data Analysis Result of Rock Images

- Binary Image → Grayscale Image → Sequence of Complexes → Persistence diagrams
- The results represent different characteristics of rock structure and connectivity
  - Size of pores and grains
  - Pore throat radius
  - Shape of pores and grains

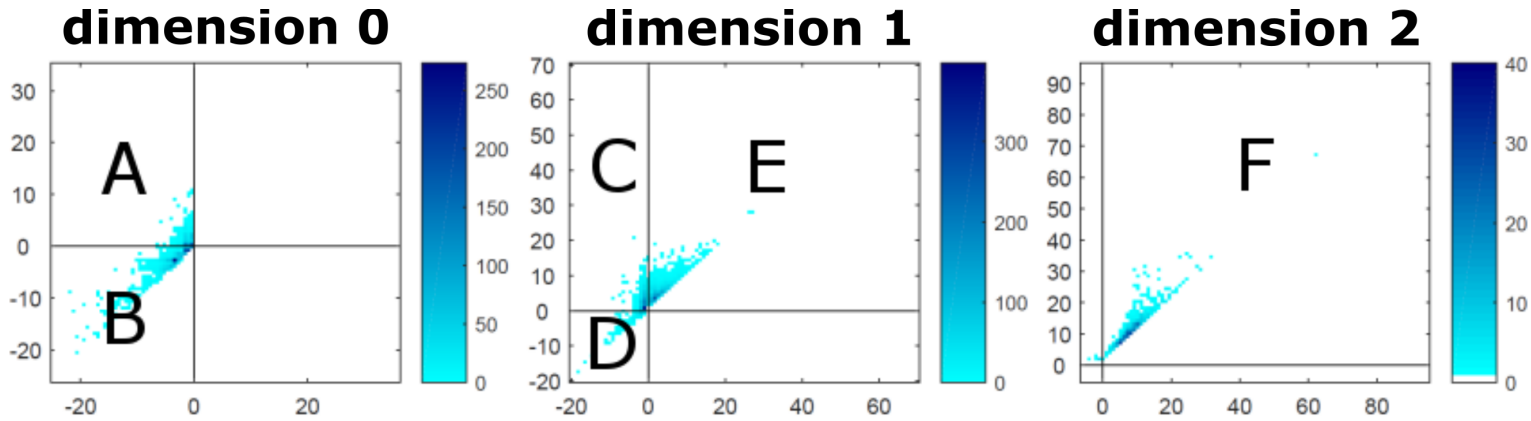

Figure: Computation results summarized as persistence diagrams

Dimension Zero: Size of Pores and Pore Throat Radius

- A: Size of disconnected pore
  - Birth (X): size of pore
  - Death (Y): distance to the nearest pore
- B: Size of connected pore and pore throat radius
  - Birth (X): size of pore
  - Death (Y): pore throat radius in the pore network

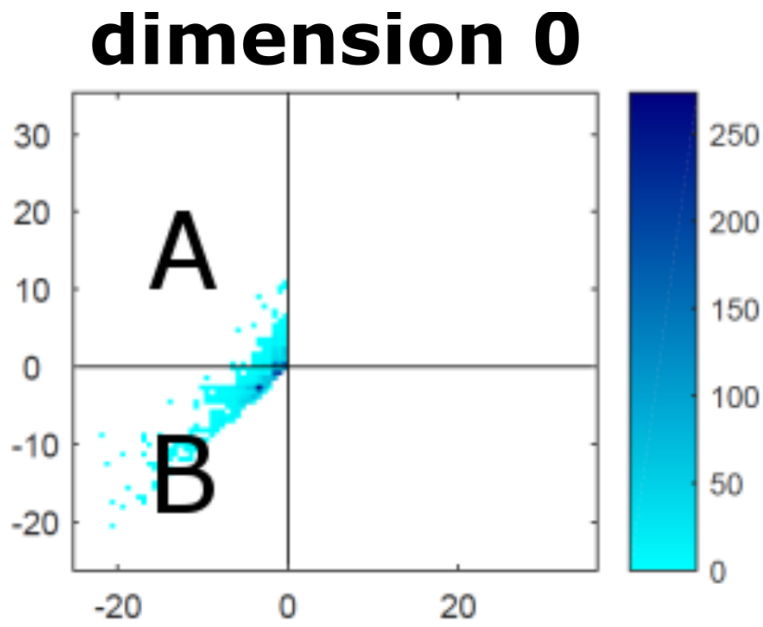

Dimension One: Shape of Pores and Grains

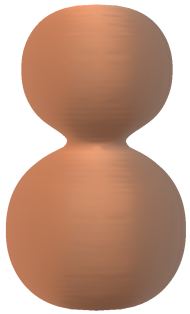

Figure: Grain contacts

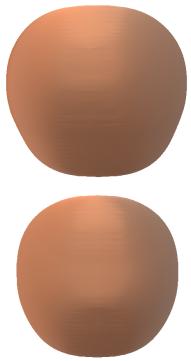

Figure: Non-convex pore structure

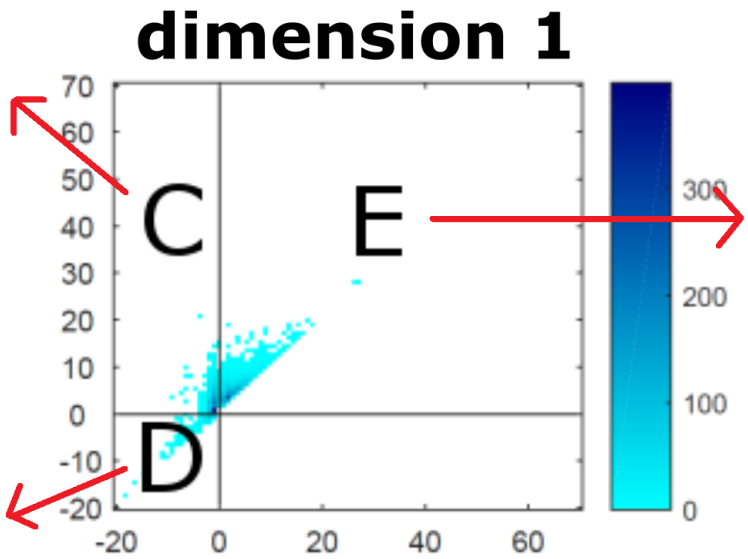

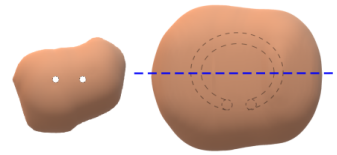

Figure: Non-convex grain structure

Dimension Two: Size of Grain

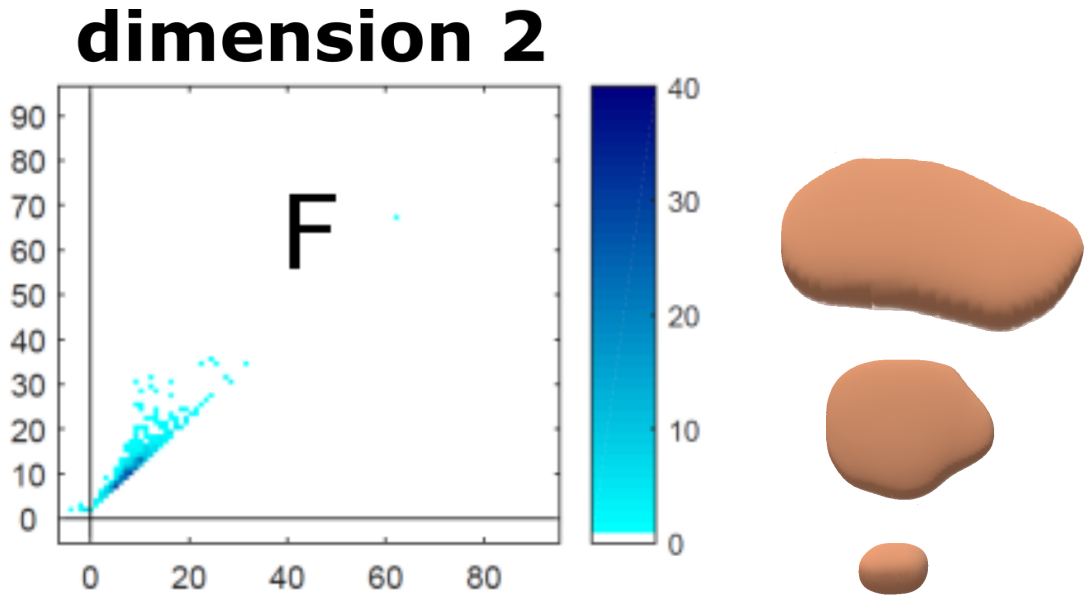

Simple Application: Strain Level Simulations

- Research question: "Can persistent homology describe deformation?"
- Use the Bentheimer strain simulation data (Moon and Andrew, 2019a)
- GeoDict (2017) finite volume simulations created a series of deformations of the Bentheimer Sandstone
- The rock was subjected to strain levels of 2%, 4%, 6%, 8%, 10%, 20%, 30%, 40%, and 50%

Rock Type	Modality	Resolution (m)	Sample	Subsamples
Bentheimer	simulation	8.9×10^{-6}	1024^3	$700 \times 600 \times 700$

Persistent Homology Describes Deformation

- zero-dimensional outputs reflect decreasing pore size
- one-dimensional outputs describe structural changes in the pores and grains
- two-dimensional outputs imply that grain sizes increase with pressure

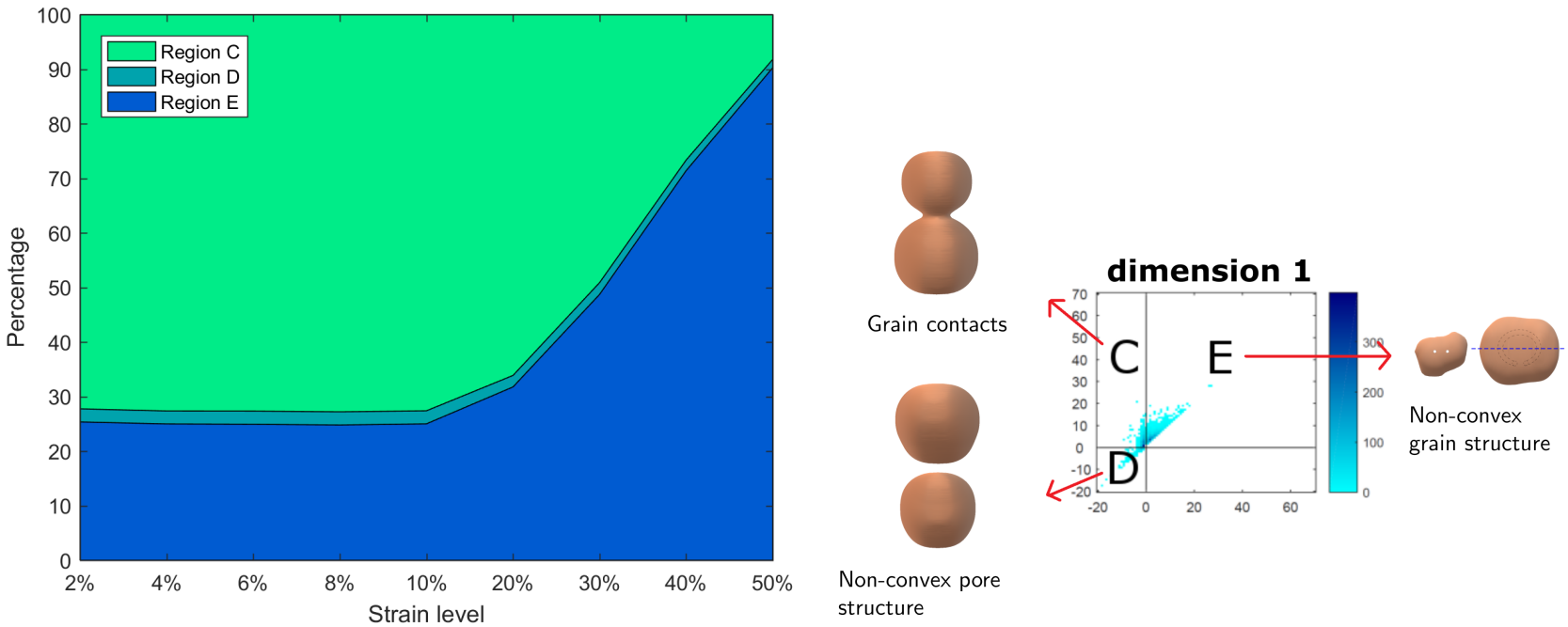

Figure: Fraction of each quadrant in one-dimensional persistence diagrams of Bentheimer Sandstone, as strain increases

Determining Sampling Size for Rock Images

- The three-dimensional rock images are expensive data to obtain
- A statistical representative elementary volume (sREV) is used to find the consistent size of materials according to the characteristics of interest
  - computationally expensive
- Can we find the sampling size for rock images?
- Underlying assumption: if the structural properties of sampled subvolumes are similar to each other, then persistence diagrams would be similar as well

Vectorized Persistence Diagrams

- Persistence diagrams are not easy to compare
- Consider persistence diagrams as an image and convert to an image vector

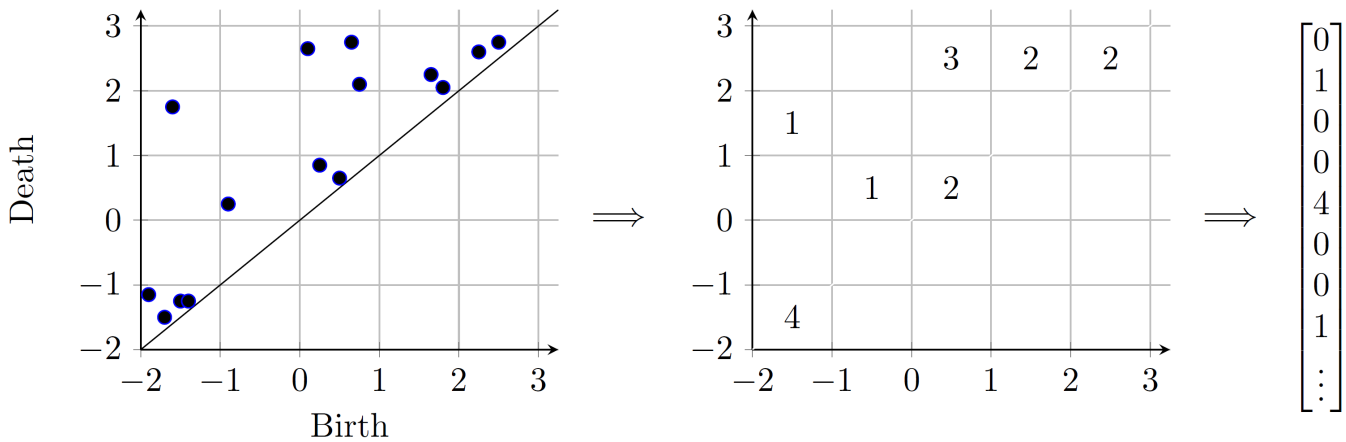

Similarity between Vectorized Persistence Diagrams

- Measure similarities between vectorized persistence diagrams using the structural similarity index (SSIM) of Wang et al. (2004)
- SSIM index 1 indicates the two images x and y are identical

$$\mathrm{SSIM}(x, y) = \frac{(2\mu_x\mu_y + C_1)(2\sigma_{xy} + C_2)}{(\mu_x^2 + \mu_y^2 + C_1)(\sigma_x^2 + \sigma_y^2 + C_2)}.$$

- The Mean SSIM (MSSIM) is the average of the SSIM values of multiple local blocks
- Local blocks that have a non-zero element are used

$$\mathrm{MSSIM}_{PH}(x, \mu) = \frac{1}{\#\{k|\mu_k \neq 0\}} \sum_{i \in \{k|\mu_k \neq \mathbf{0}\}} \mathrm{SSIM}(x_i, \mu_i).$$

Real Applications: Datasets

- Selma Chalk data (Yoon and Dewers, 2013)
- Three sandstones data (Moon and Andrew, 2019b)

Rock Type	Modality	Resolution (m)	Sample	Subsamples
Selma Chalk	FIB-SEM	15.6×10^{-9}	$930 \times 520 \times 962$	150^3, 300^3, 400^3, 500^3, $600 \times 520 \times 600$, $765 \times 520 \times 962$
Bentheimer	XRM	8.9×10^{-6}	1024^3	$700 \times 600 \times 700$
Doddington	XRM	5.4×10^{-6}	1024^3	700^3
Rotleigend	XRM	2.0×10^{-6}	1024^3	$700 \times 700 \times 980$

Application to Rock Images

- Sampling sizes of rocks are determined considering their structure and connectivity
- Compute SSIM of the mean persistence diagram and persistence diagrams for different sized subvolumes and report their mean SSIM.
- Thresholds to used: 0.95 (strict) and 0.9 (weak)

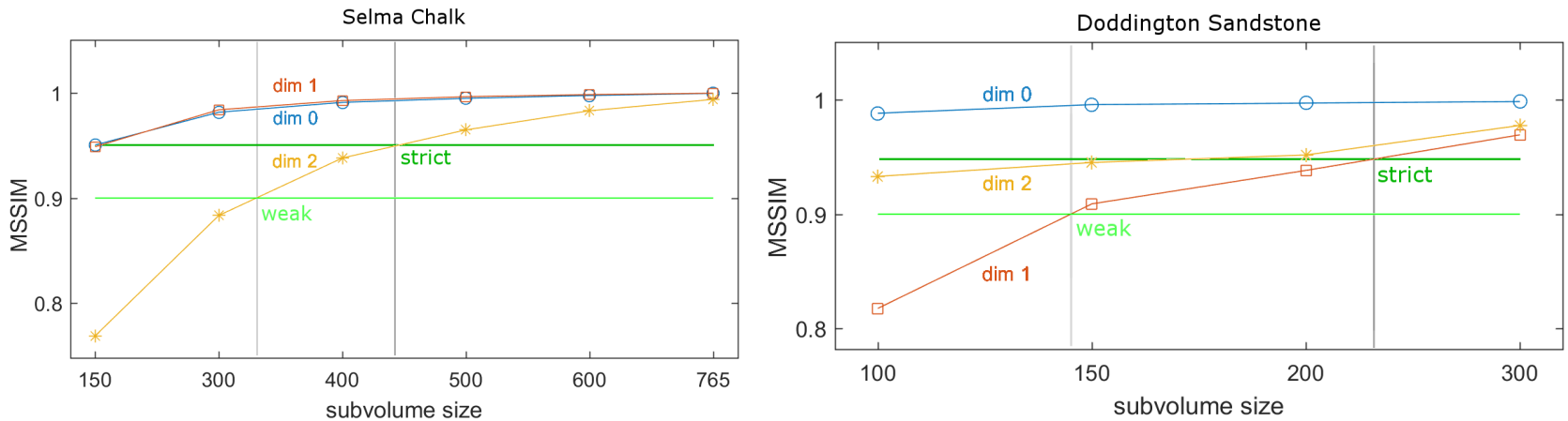

Figure: Mean SSIM of Selma chalk (left) and Doddington sandstone (right) subvolumes

Predicting Geophysical Properties

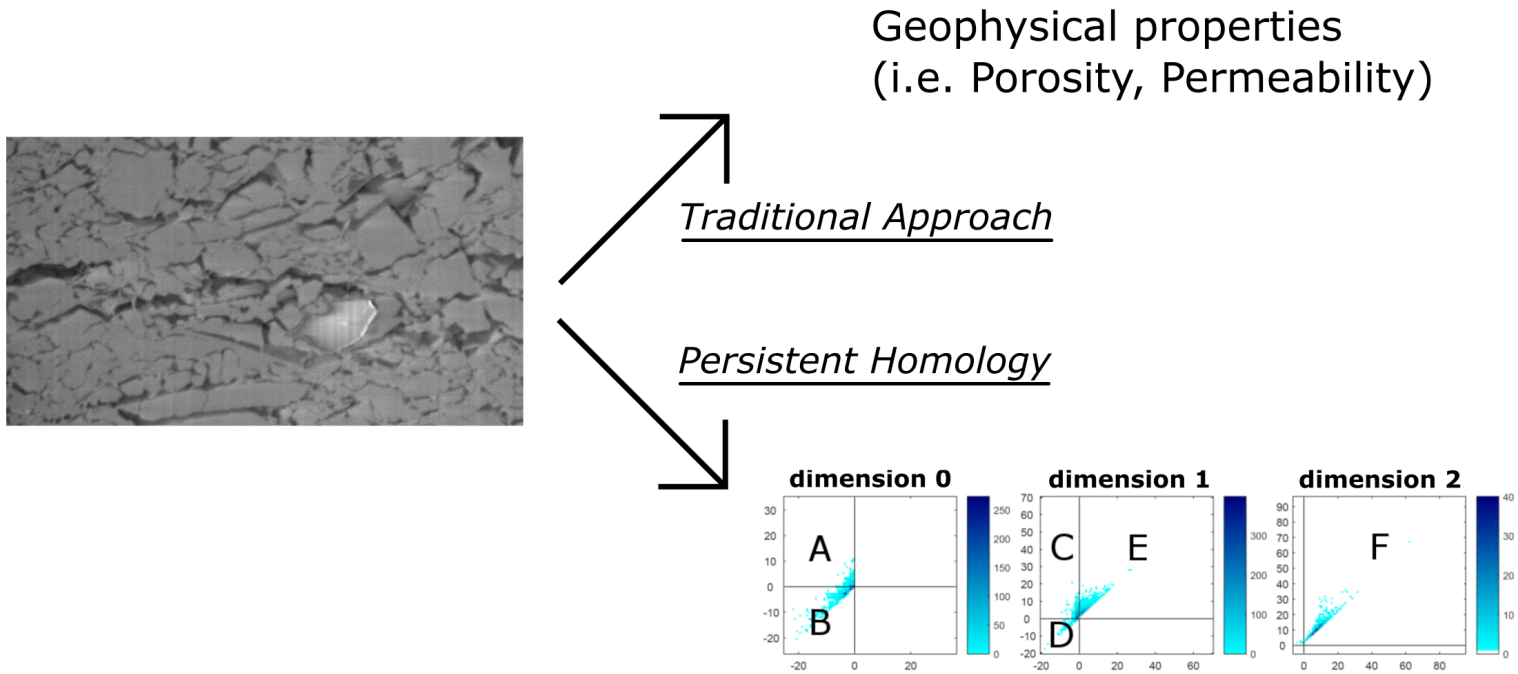

- Fit a statistical model to link persistent homology computation result with geophysical characteristics

Feature Extraction and Dimension Reduction: PCA

- Principal component analysis (PCA)

$$
\begin{aligned}
& i^{th} \text{ dimension } k \text{ persistence diagram} \\
& -\text{mean persistence diagram} \\
= \quad & c_{ik1} * PC_{k1} + c_{ik2} * PC_{k2} + \cdots + c_{ikn} * PC_{kn}
\end{aligned}
$$

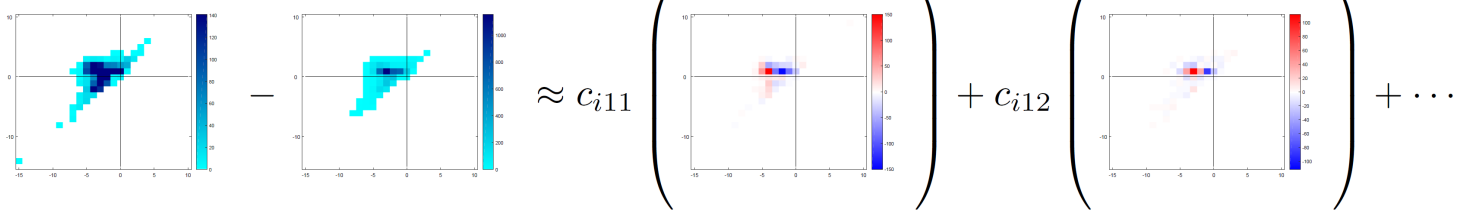

- Input variables of models: set of weights
- Vector $v_i = \{c_{i01}, c_{i02}, \cdots, c_{i2n}\}$ summarizes the i^{th} rock

Penalized Regression: LASSO

- For n rock samples, we obtain $3n$ weights; "small n large p" case

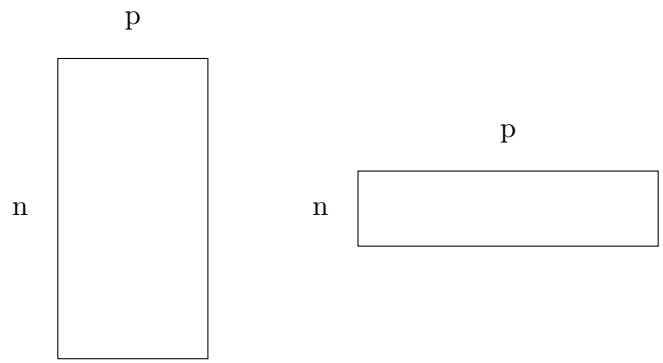

Figure: "large n small p" vs. "small n large p" data

- LASSO is the penalized regression models that give a L_1 penalty

$$\min_{\beta}\{||y - X\beta||_2^2 + \gamma||\beta||_1\}.$$

- The proposed model is

$$y = \text{geophysical property} \sim f_{LASSO}(\text{PCA weights})$$

Predictions using Selma Chalk Data (1)

- Use three sizes of subvolumes ($150^3, 300^3$ and 400^3) of Selma Chalk Data from Yoon and Dewers (2013)
- The ratio of training, validation, and test sets is 60%, 20% and 20%
- Compared the LASSO model with three models
  - (Intercept) average of y
  - (LR) linear regression model using two x variables, porosity and specific surface area
  - (PCA) linear regression model using nine weights that correspond to the principal components that have the largest eigenvalues

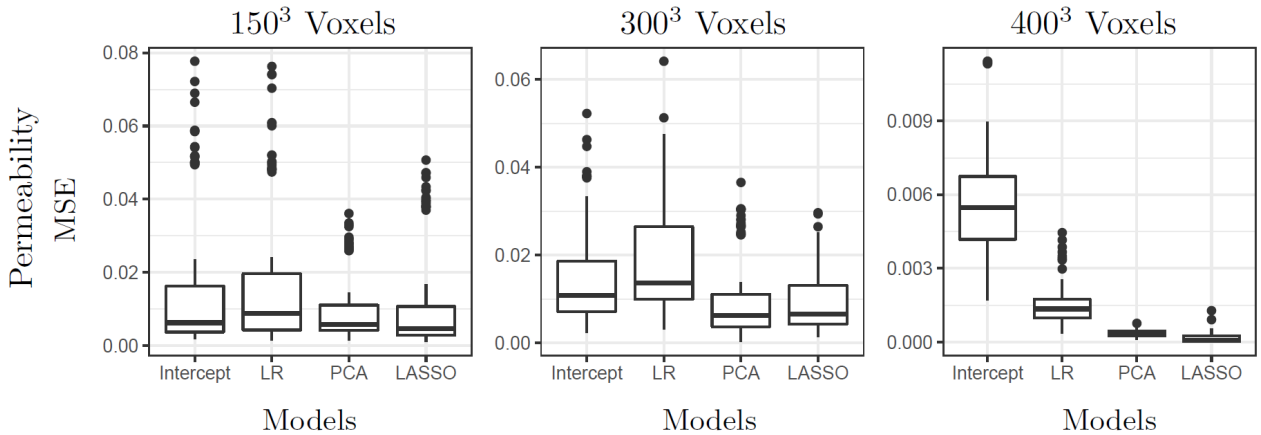

Figure: Permeability prediction results of three subvolumes

Predictions using Selma Chalk Data (2)

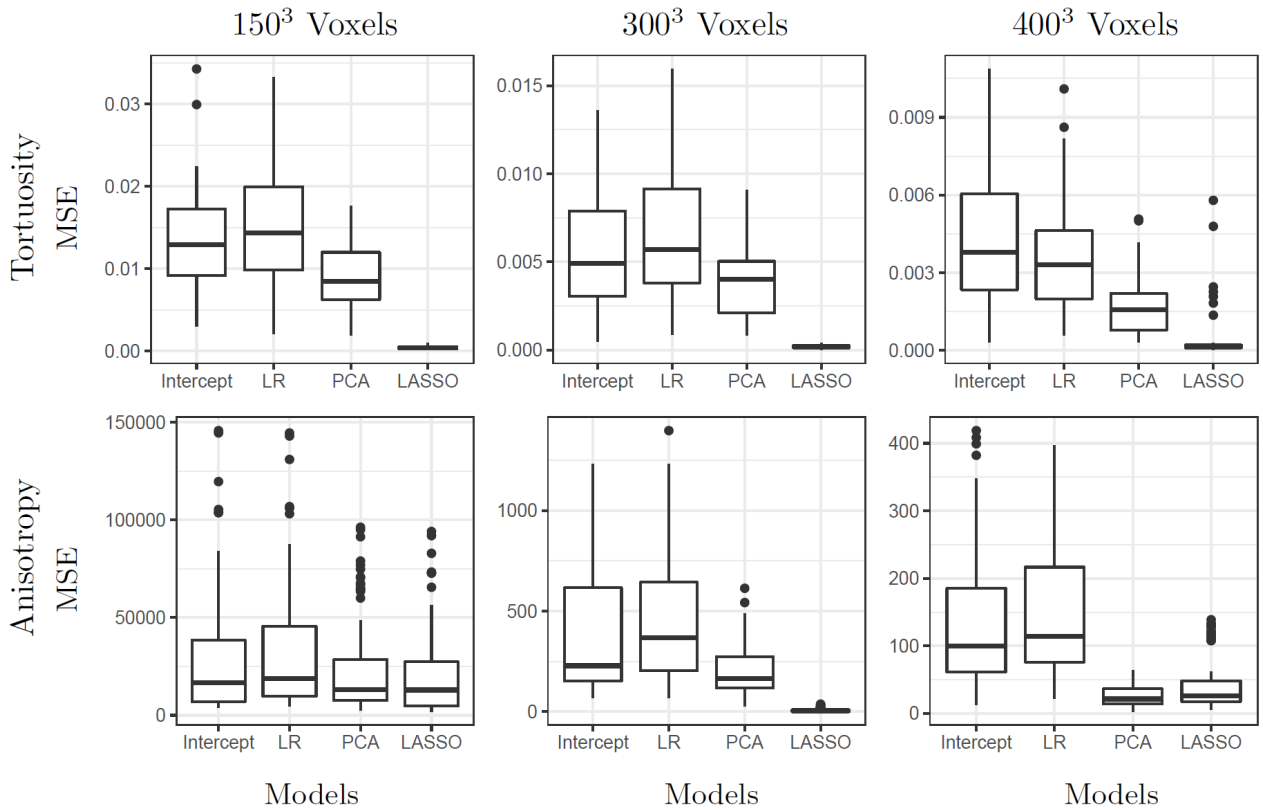

Figure: Tortuosity and anisotropy prediction results of three subvolumes

- Predict geophysical properties using a small number of rock samples

Summary

- Topological data analysis provides a tool to analyze shape/structure of data
- We propose a rock image analysis pipeline using topological data analysis
  - Hypothesis test to compare samples
  - Suggest a method to select an appropriate sampling size for porous materials
  - Predict geophysical properties using a small number of rock samples

Outline

Pathology Images and Preprocessing

- Lung cancer is one of the most deadly cancers and adenocarcinoma that accounts for about 40% of all lung cancers
- We use 247 pathology images of 143 lung adenocarcinoma patients in National Lung Screening Trial (NLST) data
- Pixels are segmented into tumor, normal, and empty regions using a deep convolutional neural network by Wang et al. (2018)

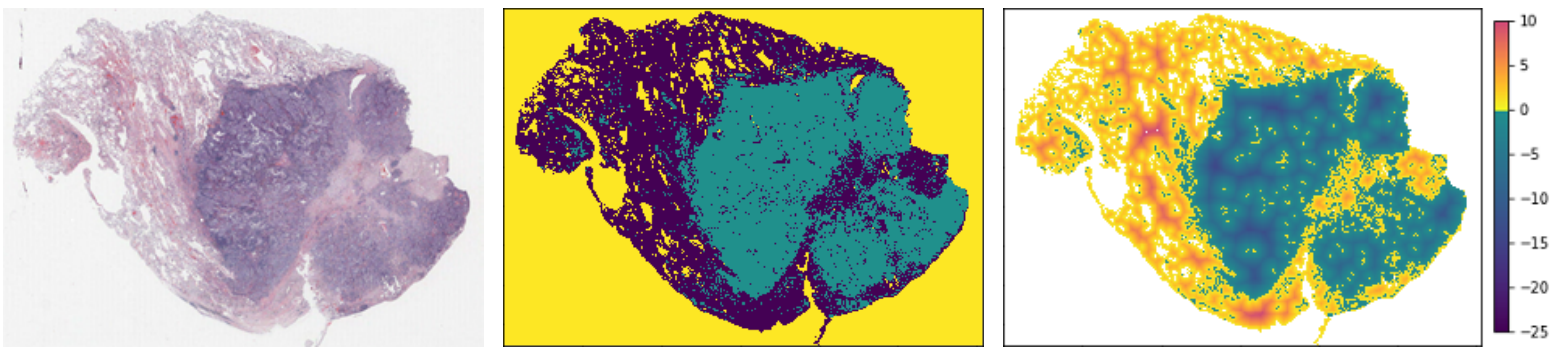

Figure: Denoised three-class pathology image and its SEDT-3

Homology of Ternary Image Data?

- Ternary image → Multiscale image
- We propose the Signed Euclidean Distance Transform for ternary image (SEDT-3)
  - Tumor – Negative vs. Normal – Positive vs. Empty – Infinite
  - Euclidean distance to the nearest the other phase pixel

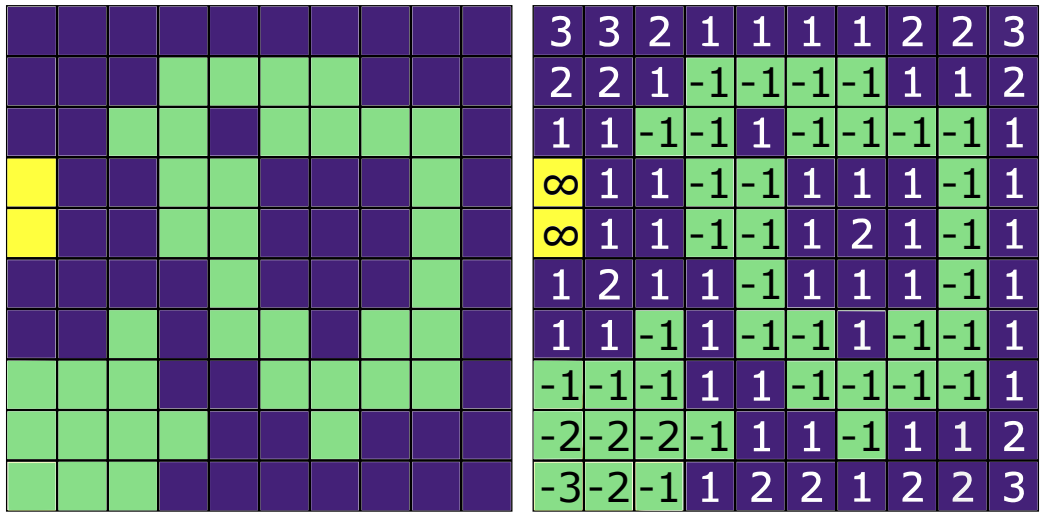

Figure: Ternary image and its signed taxicab distance transform

Constructing Complex

- Multiscale image $\rightarrow$ Sequence of complexes
- Construct complex using the SEDT-3 value: pixels whose SEDT-3 values are smaller than or equal to ϵ are used
- Start in the tumor pixels (negative), moving up to the normal pixels (positive)
- The empty pixels are not used to construct complexes

3	3	2	1	1	1	1	2	2	3
2	2	1	-1	-1	-1	-1	1	1	2
1	1	-1	-1	1	-1	-1	-1	-1	1
∞	1	1	-1	-1	1	1	1	-1	1
∞	1	1	-1	-1	1	2	1	-1	1
1	2	1	1	-1	1	1	1	-1	1
1	1	-1	1	-1	-1	1	-1	-1	1
-1	-1	-1	1	1	-1	-1	-1	-1	1
-2	-2	-2	-1	1	1	-1	1	1	2
-3	-2	-1	1	2	2	1	2	2	3

Constructing Complex

- Multiscale image $\rightarrow$ Sequence of complexes
- Construct complex using the SEDT-3 value: pixels whose SEDT-3 values are smaller than or equal to ϵ are used
- Start in the tumor pixels (negative), moving up to the normal pixels (positive)
- The empty pixels are not used to construct complexes

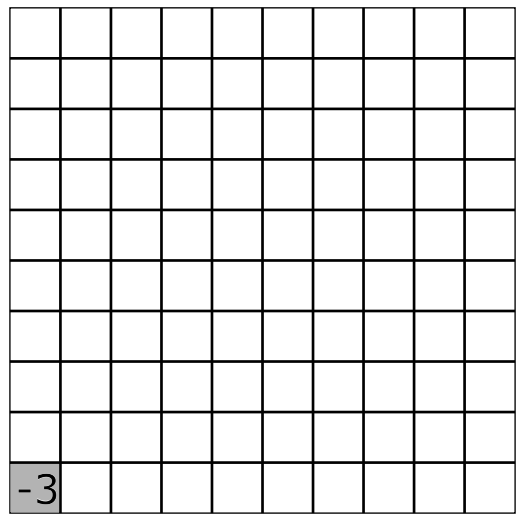

Figure: $\epsilon = -3$

Constructing Complex

- Multiscale image $\rightarrow$ Sequence of complexes
- Construct complex using the SEDT-3 value: pixels whose SEDT-3 values are smaller than or equal to ϵ are used
- Start in the tumor pixels (negative), moving up to the normal pixels (positive)
- The empty pixels are not used to construct complexes

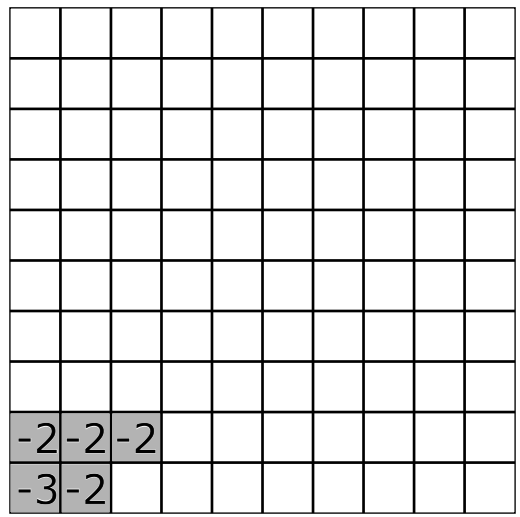

Figure: $\epsilon = -2$

Constructing Complex

- Multiscale image $\rightarrow$ Sequence of complexes
- Construct complex using the SEDT-3 value: pixels whose SEDT-3 values are smaller than or equal to ϵ are used
- Start in the tumor pixels (negative), moving up to the normal pixels (positive)
- The empty pixels are not used to construct complexes

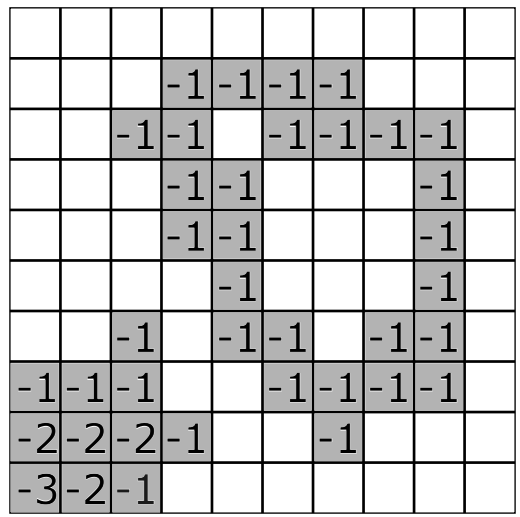

Figure: $\epsilon = -1$

Constructing Complex

- Multiscale image $\rightarrow$ Sequence of complexes
- Construct complex using the SEDT-3 value: pixels whose SEDT-3 values are smaller than or equal to ϵ are used
- Start in the tumor pixels (negative), moving up to the normal pixels (positive)
- The empty pixels are not used to construct complexes

			1	1	1	1			
		1	-1	-1	-1	-1	1	1	
1	1	-1	-1	1	-1	-1	-1	-1	1
	1	1	-1	-1	1	1	1	-1	1
	1	1	-1	-1	1		1	-1	1
1		1	1	-1	1	1	1	-1	1
1	1	-1	1	-1	-1	1	-1	-1	1
-1	-1	-1	1	1	-1	-1	-1	-1	1
-2	-2	-2	-1	1	1	-1	1	1	
-3	-2	-1	1			1			

Figure: $\epsilon = 1$

Constructing Complex

- Multiscale image $\rightarrow$ Sequence of complexes
- Construct complex using the SEDT-3 value: pixels whose SEDT-3 values are smaller than or equal to ϵ are used
- Start in the tumor pixels (negative), moving up to the normal pixels (positive)
- The empty pixels are not used to construct complexes

		2	1	1	1	1	2	2	
2	2	1	-1	-1	-1	-1	1	1	2
1	1	-1	-1	1	-1	-1	-1	-1	1
	1	1	-1	-1	1	1	1	-1	1
	1	1	-1	-1	1	2	1	-1	1
1	2	1	1	-1	1	1	1	-1	1
1	1	-1	1	-1	-1	1	-1	-1	1
-1	-1	-1	1	1	-1	-1	-1	-1	1
-2	-2	-2	-1	1	1	-1	1	1	2
-3	-2	-1	1	2	2	1	2	2	

Figure: $\epsilon = 2$

Constructing Complex

- Multiscale image $\rightarrow$ Sequence of complexes
- Construct complex using the SEDT-3 value: pixels whose SEDT-3 values are smaller than or equal to ϵ are used
- Start in the tumor pixels (negative), moving up to the normal pixels (positive)
- The empty pixels are not used to construct complexes

3	3	2	1	1	1	1	2	2	3
2	2	1	-1	-1	-1	-1	1	1	2
1	1	-1	-1	1	-1	-1	-1	-1	1
	1	1	-1	-1	1	1	1	-1	1
	1	1	-1	-1	1	2	1	-1	1
1	2	1	1	-1	1	1	1	-1	1
1	1	-1	1	-1	-1	1	-1	-1	1
-1	-1	-1	1	1	-1	-1	-1	-1	1
-2	-2	-2	-1	1	1	-1	1	1	2
-3	-2	-1	1	2	2	1	2	2	3

Figure: $\epsilon = 3$

Topological Data Analysis Result of Binary Images

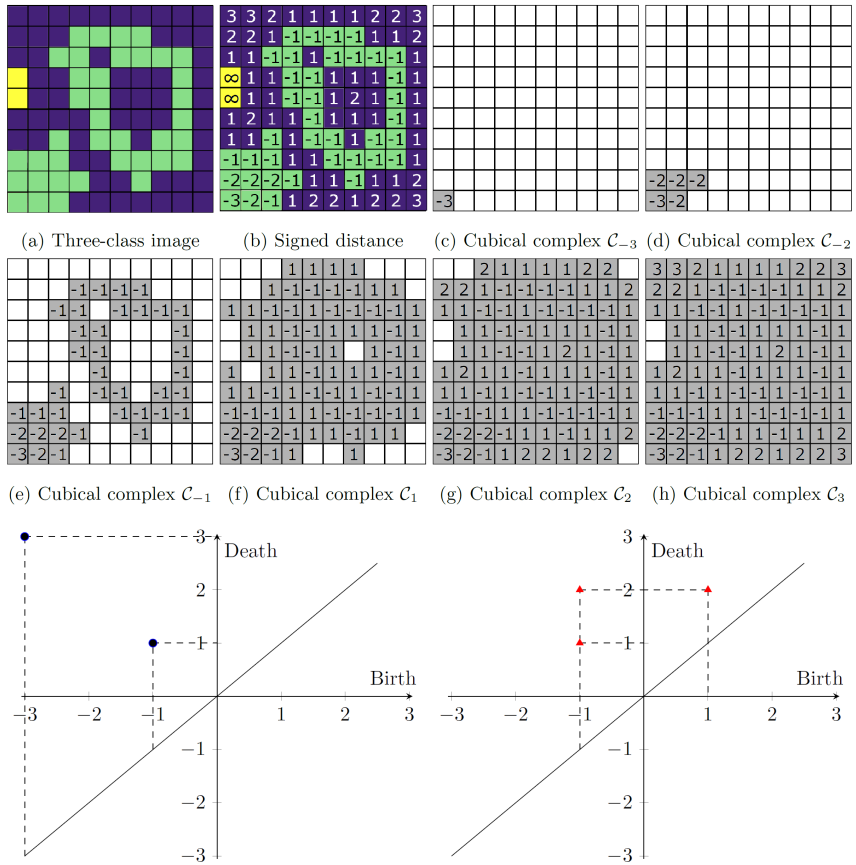

Figure: Computation results summarized as persistence diagrams

Which information can we obtain here?

Dimension Zero Features: Size and Distributions of Tumors

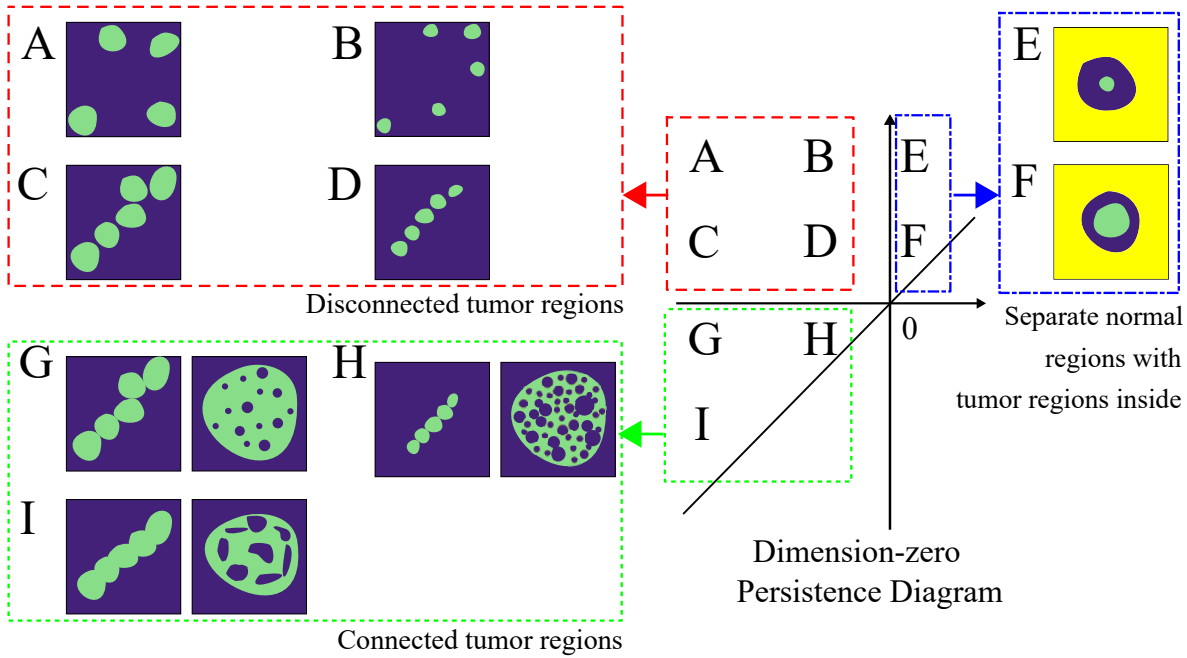

- Quadrant II (e.g., A, B, C, and D)
  - Scattered tumors
  - Birth (X): size of tumor (larger the tumor, larger the absolute birth values)
  - Death (Y): distances between tumor regions (further the tumor regions, larger the death values)

Dimension Zero Features: Size and Distributions of Tumors

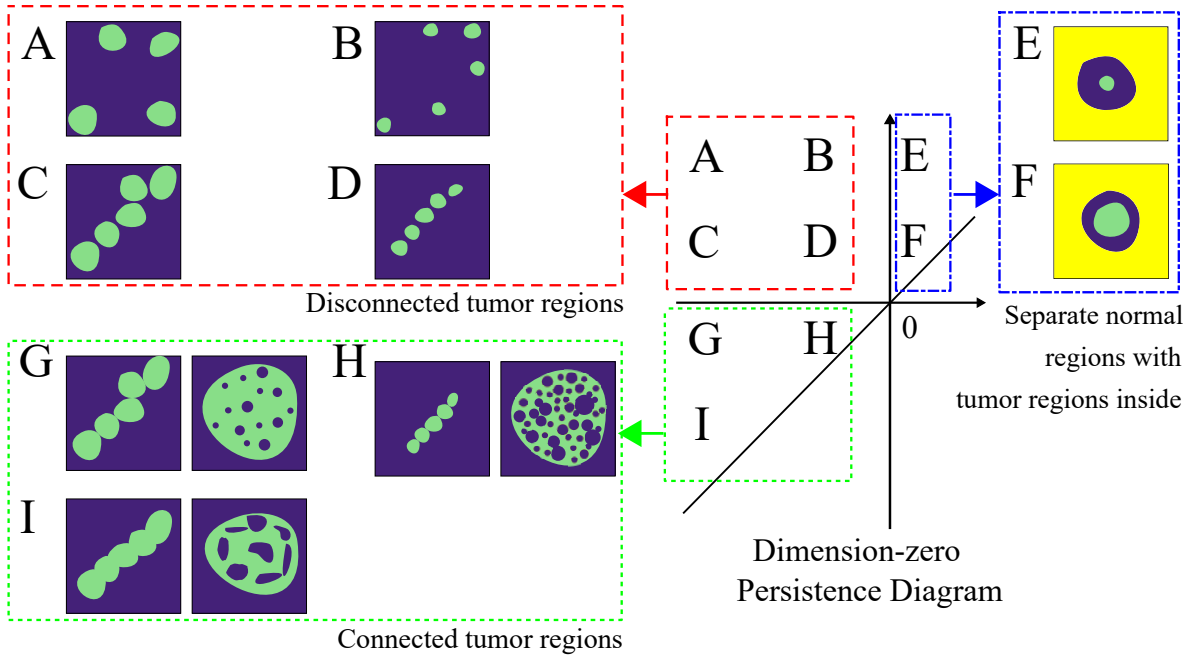

- Quadrant I (e.g., E and F)
  - Separate normal regions that include tumor regions
  - Larger the death values, thicker the normal regions

Dimension Zero Features: Size and Distributions

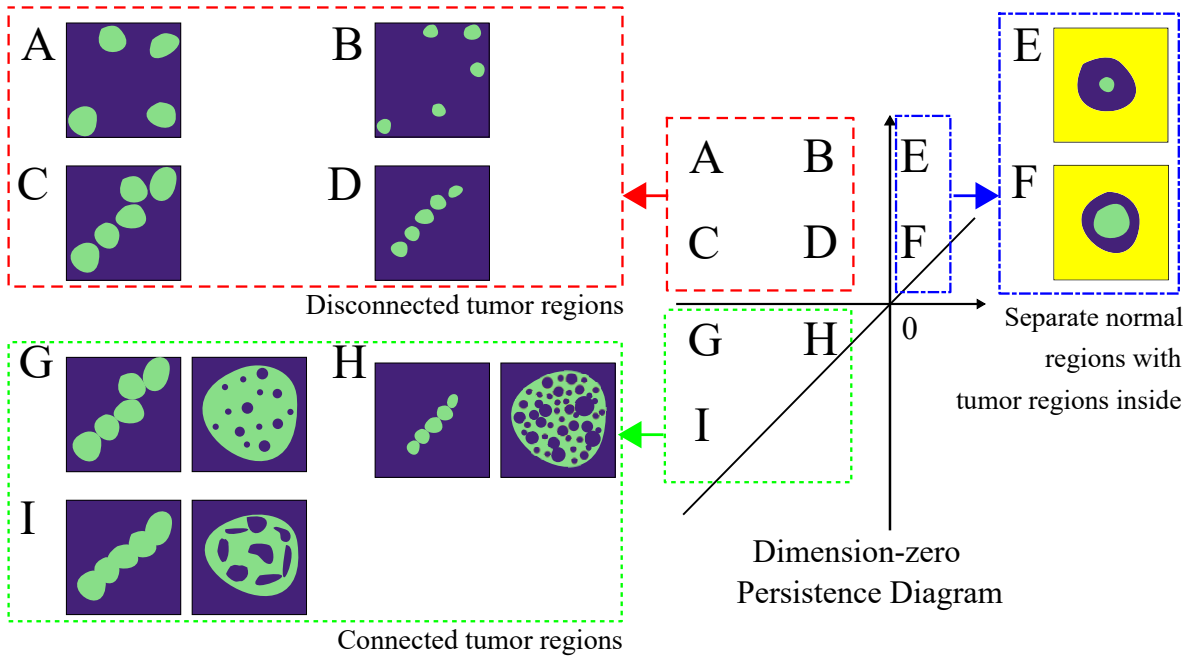

- Quadrant III (e.g., G, H, and I)
  - Connected tumor regions
  - Birth (X): size of tumor (larger the tumor, larger the absolute birth values)
  - Death (Y): contact area of two tumor regions (larger the contact areas, larger the absolute death values)

Dimension One Features: Shape

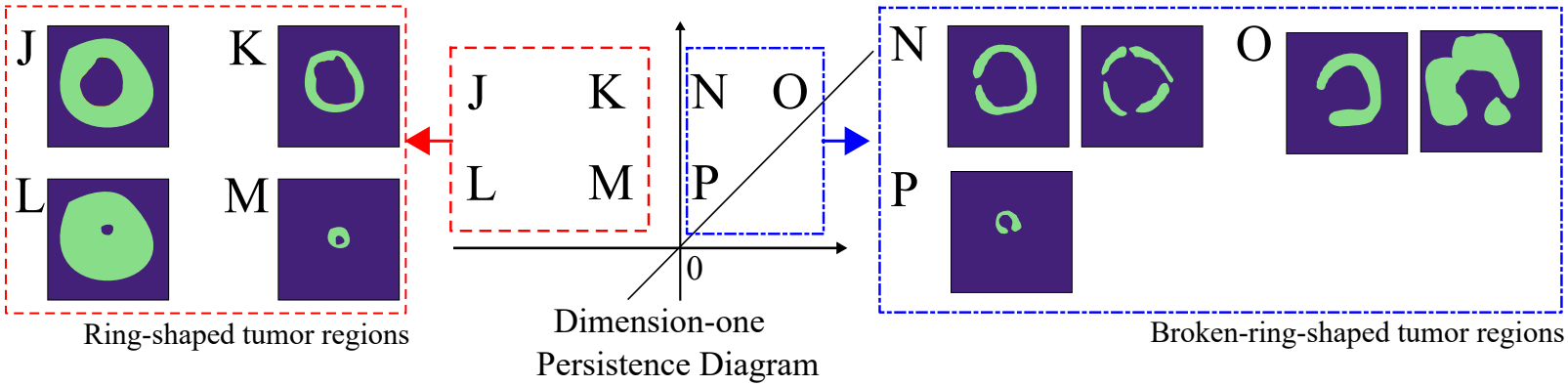

- Quadrant II (e.g., J, K, L, and M)
  - Tumor region that surrounds normal region
  - Birth (X): thickness of tumor region (thicker the tumor region, larger the absolute birth values)
  - Death (Y): size of trapped normal region (larger the normal region, larger the death values)

Dimension One Features: Shape

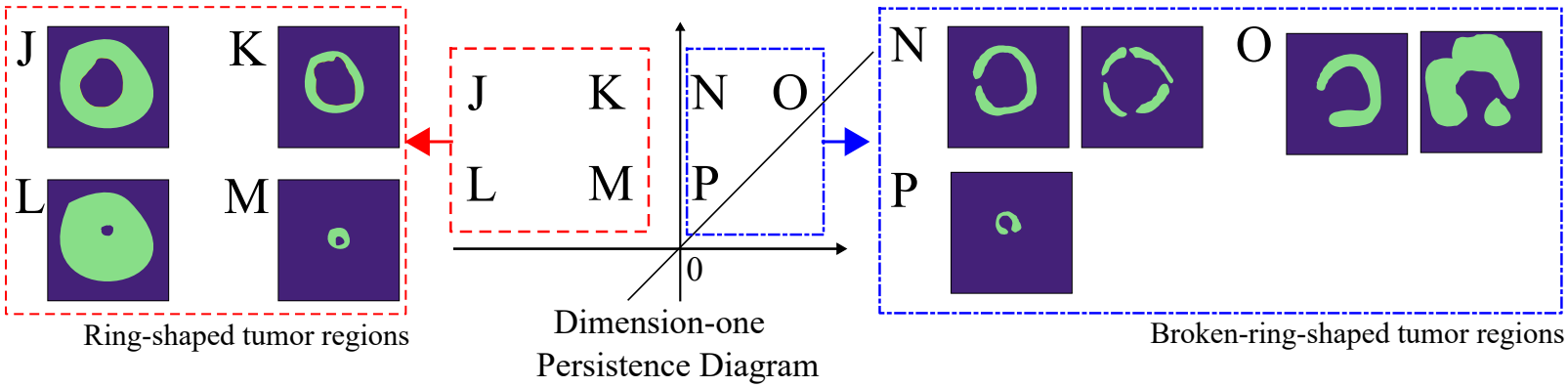

- Quadrant I (e.g., N, P, and O)
  - Broken-ring shaped tumor regions
  - Birth (X): size of pore
  - Death (Y): distance to the nearest pore

Additional Notes on Topological Features

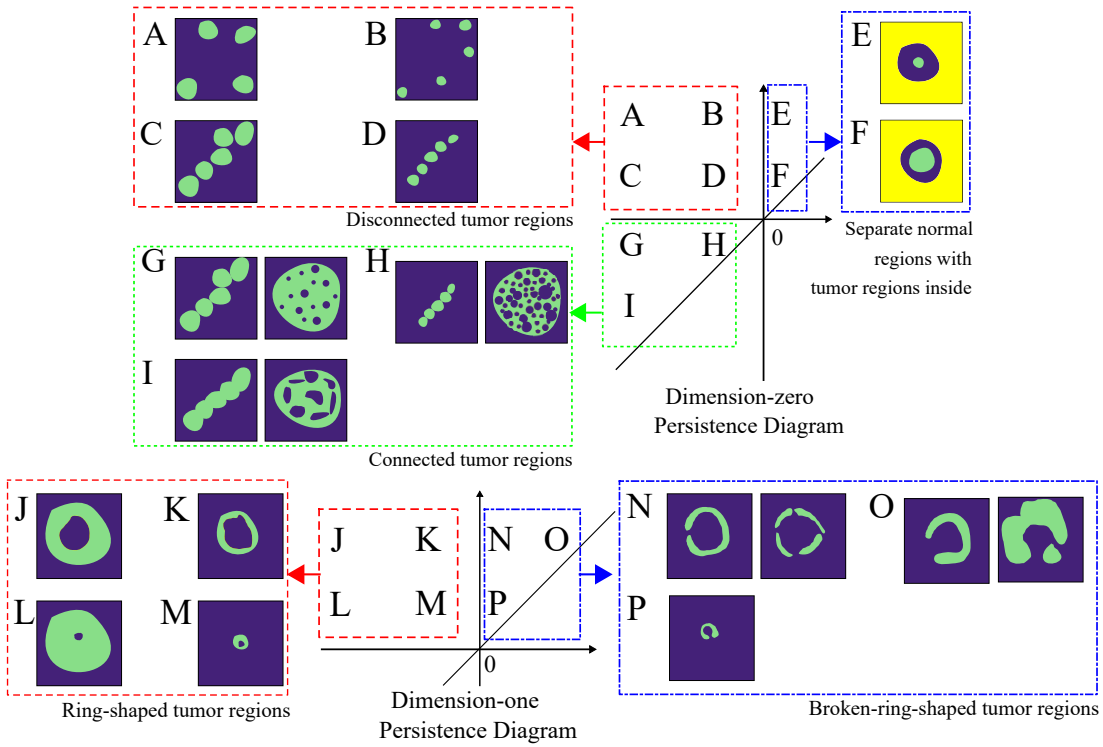

- The size of features is measured by the radius of the largest circle that can be placed inside of it.
- Dimension zero and one features are not exclusive; the pixels used to construct dimension zero features can be used to build dimension one feature and vice versa.

Functional Survival Model

- Predict survival risks of patients using clinical variables and persistent homology shape features (i.e., persistence functions X^0 and X^1)
- Functional Cox proportional-hazards (FCoxPH) model

$$h(t) = h_0(t) \exp\left(Z^T\gamma + \int X^0(u)\alpha(u)du + \int X^1(v)\beta(v)dv \right).$$

where h_0 is the baseline hazard function, $t \in [0, \tau]$ for $0 < \tau < \infty$, $Z = (z_1, \ldots, z_p)^T$ is a p-dimensional scalar predictor, and X^0 and X^1 are functional topological shape data

- Use both scalar variable Z and two functional predictors X^0 and X^1

FCoxPH Model with Selected FPCs

- Dimension reduction of functional data is required due to their infinite dimensions
  - Functional data is approximated by the functional principal component (FPC) analysis with q and r selected number of FPCs

$$X_i^0 \approx \mu^0(u) + \sum_{j=1}^{q} \xi_{ij}\phi_j(u) \text{ and } X_i^1 \approx \mu^1(v) + \sum_{k=1}^{r} \zeta_{ik}\pi_k(v)$$

- The FCoxPH model can be approximated as

$$h_i(t) \approx h_0^*(t) \exp\left(Z_i^T\gamma + \sum_{j=1}^{q} \xi_{ij}\alpha_j + \sum_{k=1}^{r} \zeta_{ik}\beta_k \right)$$

- Use Akaike Information Criterion (AIC) to select the number of FPCs
  - $AIC(q,r) = 2(q+r) - 2\log\{L(\hat{\gamma}_1, \ldots, \hat{\gamma}_p, \hat{\alpha}_1, \ldots, \hat{\alpha}_q, \hat{\beta}_1, \ldots, \hat{\beta}_r | q, r)\}$

Two Survival models

1. Cox regression (CoxPH) model
   - Scalar (clinical) predictors: age, sex, smoking status, stage of cancer (I to IV), and tumor size
2. Functional Cox regression (FCoxPH) model
   - Scalar (clinical) predictors: age, sex, smoking status, stage of cancer (I to IV), and tumor size
   - Functional (topological) predictors: three FPCs are selected $q = 1$ and $r = 2$ by AIC.

Estimated Survival Models

- The overall p-values of the Wald tests for global statistical significance are 2×10^{-4} for the CoxPH model and 3×10^{-7} for the FCoxPH model
- The chi-square test indicates that the topological features are a strong signal (p-value $= 1 \times 10^{-13}$)

	CoxPH model				FCoxPH model			
	coef.	exp(coef.)	SE	p-value	coef.	exp(coef.)	SE	p-value
Age	0.084	1.088	0.023	**0.007**	0.083	1.087	0.024	**0.013**
Smoker vs. non-smoker	-0.067	0.935	0.262	0.831	-0.253	0.776	0.234	0.426
Female vs. male	0.081	1.085	0.235	0.803	0.088	1.092	0.242	0.791
Tumor size	0.000	1.000	0.000	0.084	<0.001	1.000	<0.001	0.572
Stage II vs. stage I	0.545	1.725	0.382	0.366	0.477	1.611	0.390	0.432
Stage III vs. stage I	1.195	3.304	0.270	**0.002**	1.170	3.222	0.277	**0.002**
Stage IV vs. stage I	1.442	4.227	0.342	**0.002**	1.424	4.152	0.346	**0.003**
Dimension 0, 1^{st} FPC	-	-	-	-	0.005	1.005	0.001	<**0.001**
Dimension 1, 1^{st} FPC	-	-	-	-	<0.001	1.001	<0.001	**0.002**
Dimension 1, 2^{nd} FPC	-	-	-	-	-0.002	0.998	<0.001	<**0.001**

Estimated Coefficient Functions and Clinical Implications

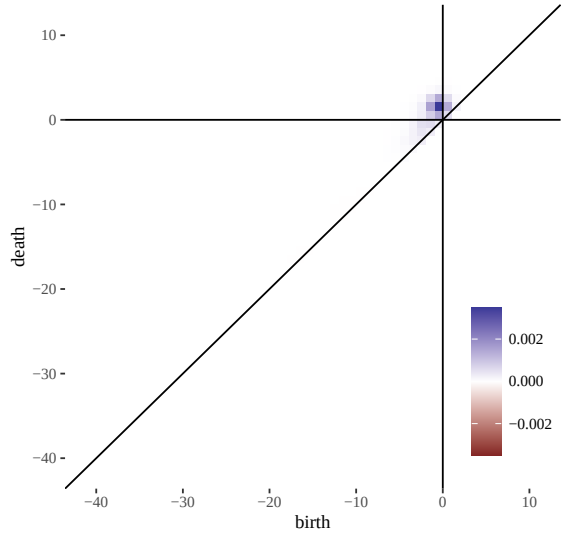

(a) Estimated dimension zero functional coefficient $\hat{\alpha}(u)$

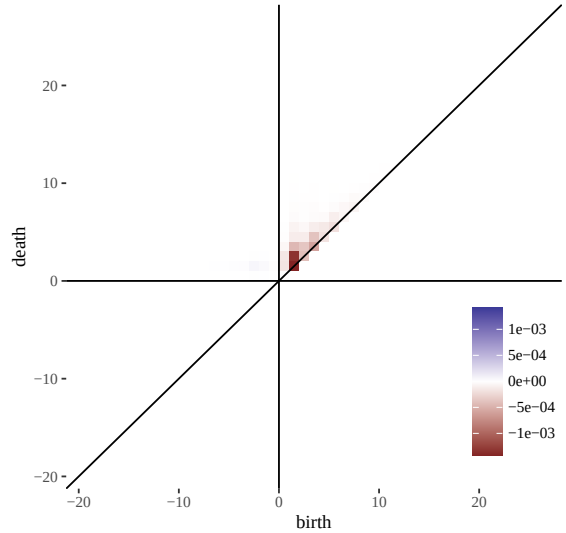

(b) Estimated dimension one functional coefficient $\hat{\beta}(v)$

- Estimated coefficient functions show which topological features are related with the survival risks
  - Blue-colored areas: aggressive tumor patterns
  - Red-colored areas: less-aggressive tumor patterns
- These results coincide with the existing findings on how tumor shapes associate with tumor progression and patient survival

Prediction using Cross-Validation

- Predict the risk scores using the leave-one-out cross-validation (LOOCV) for two models and assign the patients into 71 high-risk and 72 low-risk patients groups
- The p-value of the log-rank test of the FCoxPH model is 3×10^{-7}, which is smaller than that of the CoxPH model 5×10^{-5}.

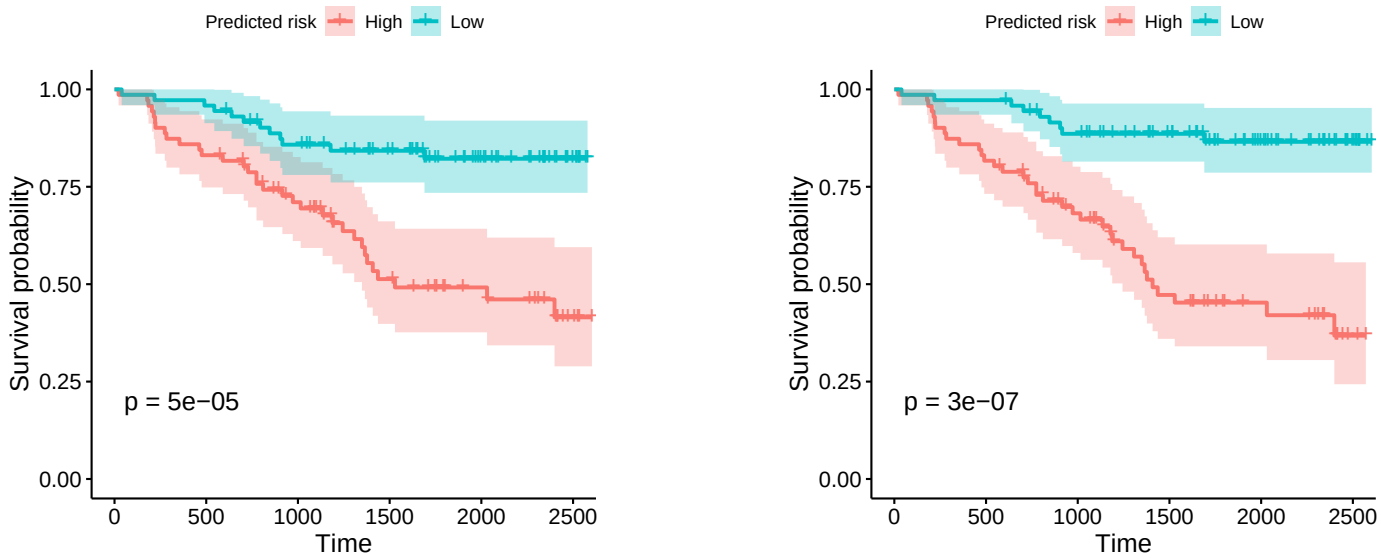

(a) CoxPH model (b) FCoxPH model

Figure: The Kaplan–Meier plots for the high- and low-risk groups

Glioblastoma MRI Data

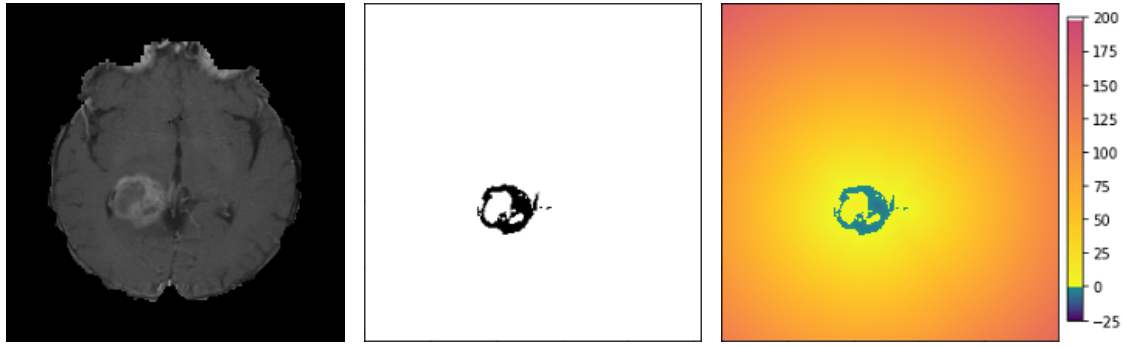

- Glioblastoma multiforme (GBM) is the most common malignant grade IV brain tumor
- The rapid outward growth of GBM develops necrosis, and most GBM cases show a ring-shaped enhancement
- We use 77 GBM patients' MRIs from The Cancer Imaging Archive and clinical data from The Cancer Genome Atlas
- MRI Images are segmented using the Medical Imaging Interaction Toolkit with augmented tools for segmentation
- Scalar predictors: age, gender, Karnofsky performance score (KPS)

Estimated Survival models

- Four FPCs ($q = 1$ and $r = 3$) are selected by AIC
- The overall p-values of the Wald tests are 0.02 for the CoxPH model and 6×10^{-4} for the FCoxPH model
- The p-value of the chi-square test of degrees of freedom four is 2×10^{-4}, suggesting that the topological features are a strong signal.

	CoxPH model				FCoxPH model			
	coef.	exp(coef.)	SE	p-value	coef.	exp(coef.)	SE	p-value
Age	0.030	1.030	0.013	**0.024**	0.035	1.036	0.013	**0.006**
Female vs. male	-0.030	0.744	0.311	0.340	-0.345	0.708	0.312	0.269
KPS	-0.021	0.980	0.010	**0.048**	-0.009	0.991	0.011	0.454
Dimension 0, 1st FPC	-	-	-	-	0.002	1.002	0.117	0.990
Dimension 1, 1st FPC	-	-	-	-	0.161	1.175	0.115	0.163
Dimension 1, 2nd FPC	-	-	-	-	0.045	1.175	0.084	0.597
Dimension 1, 3rd FPC	-	-	-	-	-0.305	0.737	0.128	**0.018**

Estimated Coefficient Functions and Clinical Implications

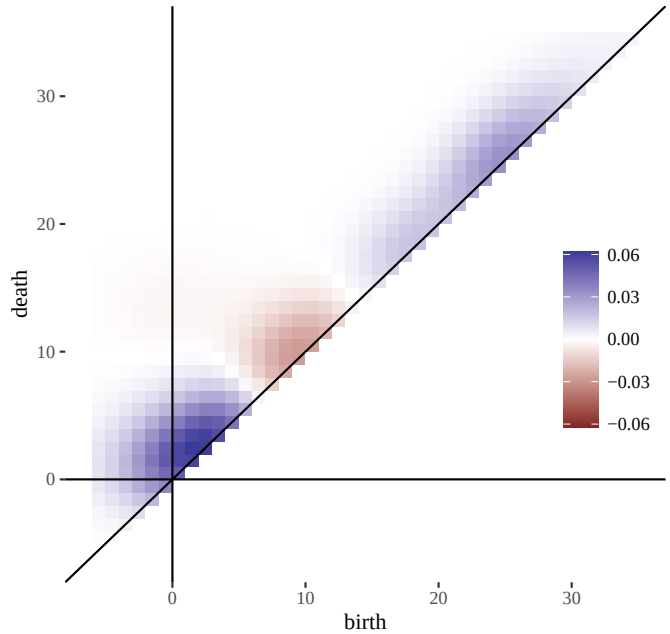

Figure: Estimated dimension one functional coefficient $\hat{\beta}(v)$

- Blue-colored areas: tumor patterns positively related with risks
- Red-colored areas: tumor patterns negatively related with risks

Prediction using Cross-Validation

- Compare three models: Gaussian Process (GP) of Crawford et al. (2020), CoxPH, and FCoxPH models
- Predict the risk scores using the LOOCV and assign the patients into 38 high-risk and 39 low-risk patients groups
- The p-values of the log-rank tests are 0.0069 for the FCoxPH model and 0.17 for the CoxPH model

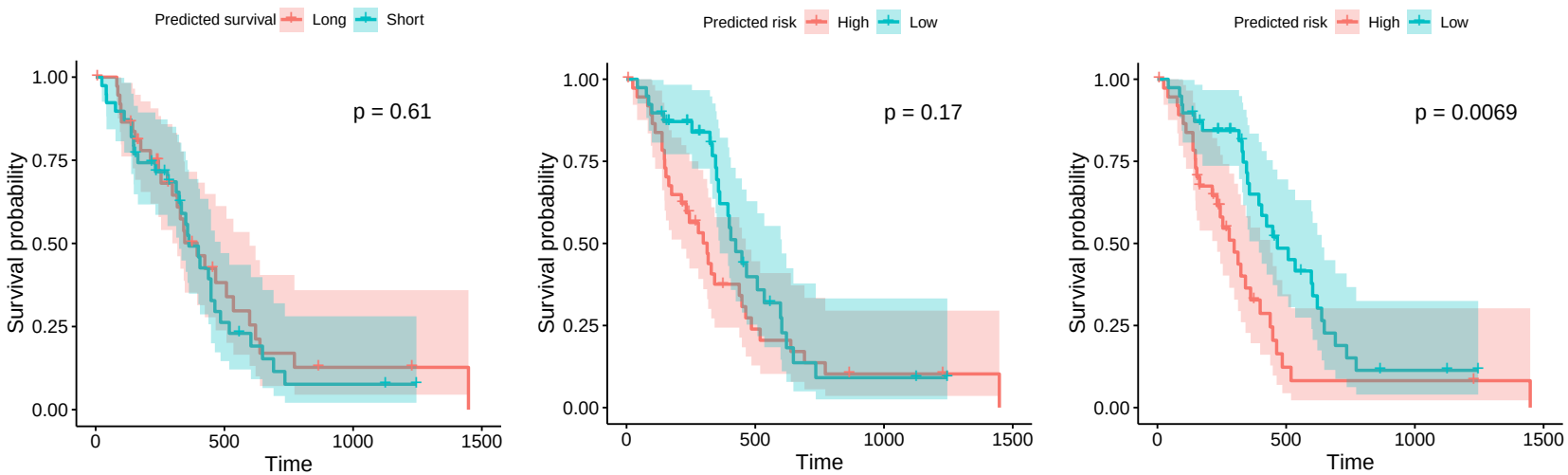

(a) GP model (b) CoxPH model (c) FCoxPH model

Figure: The Kaplan–Meier plots for the high- and low-risk groups

Conclusions

- Propose a new tumor shape summary statistic of medical images using topological features
- The topological features are shown to have a significant non-zero effect on the hazard function; This suggests that the topological features well summarize tumor aggressiveness
- The proposed model provides interpretable topological shape features while considering right-censored observations

Outline

For more detailed review, see Ravishanker and Chen (2019).

Morse Function

- Time series data → Morse function

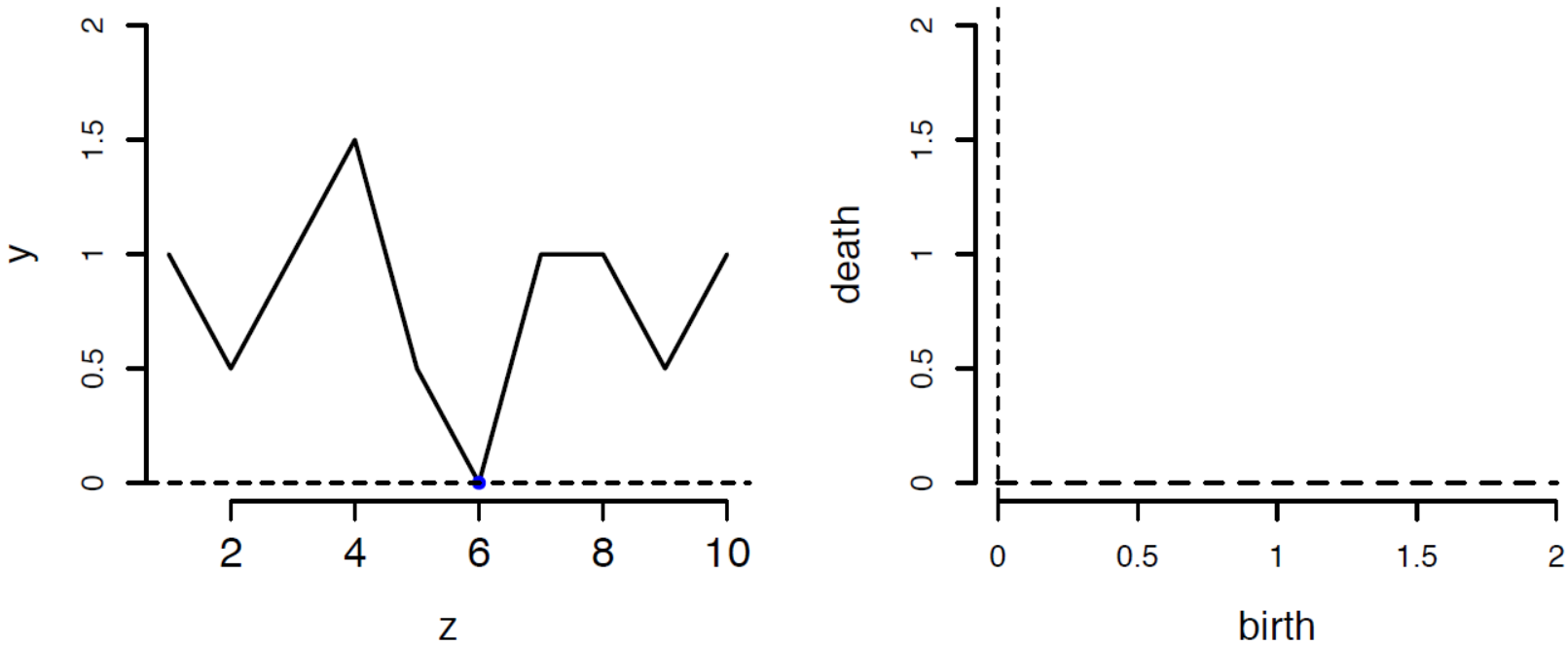

Figure: Figures from Ravishanker and Chen (2019)

Morse Function

- Time series data $\rightarrow$ Morse function

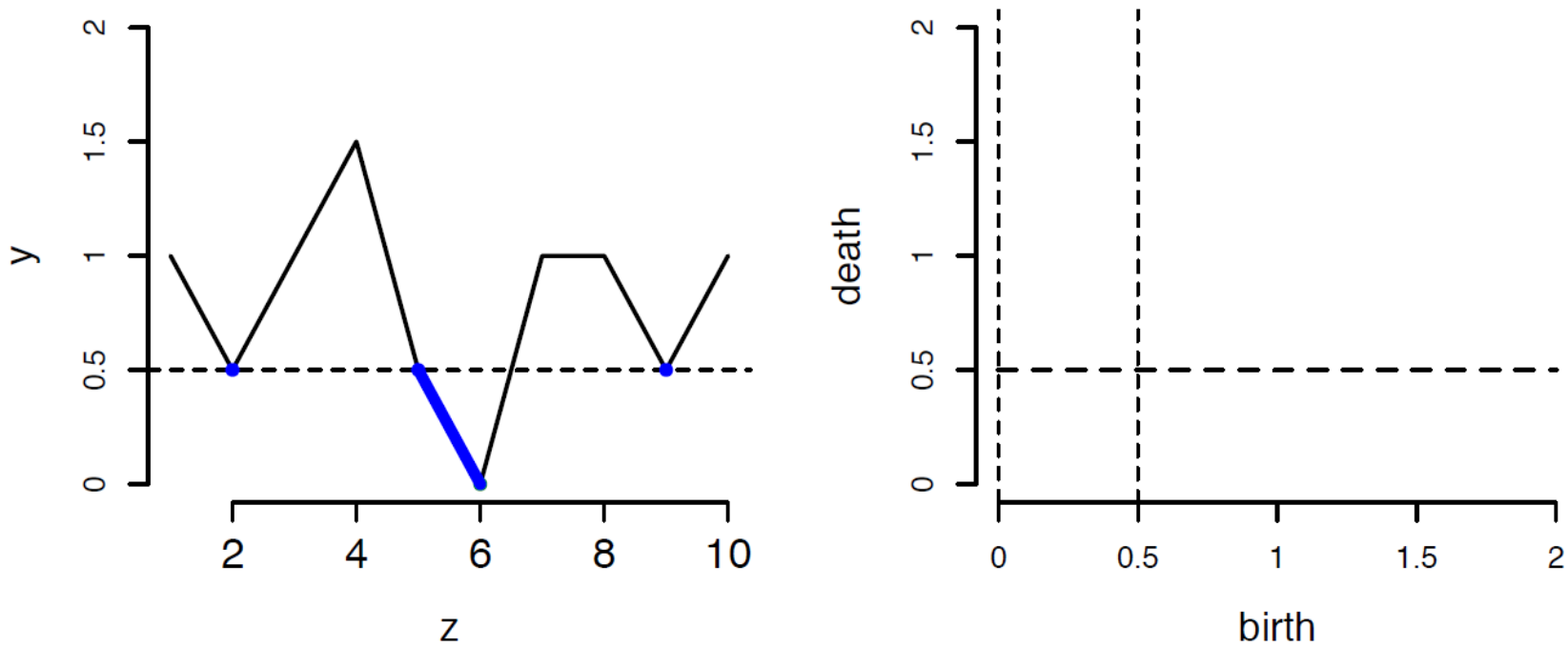

Figure: Figures from Ravishanker and Chen (2019)

Morse Function

- Time series data $\rightarrow$ Morse function

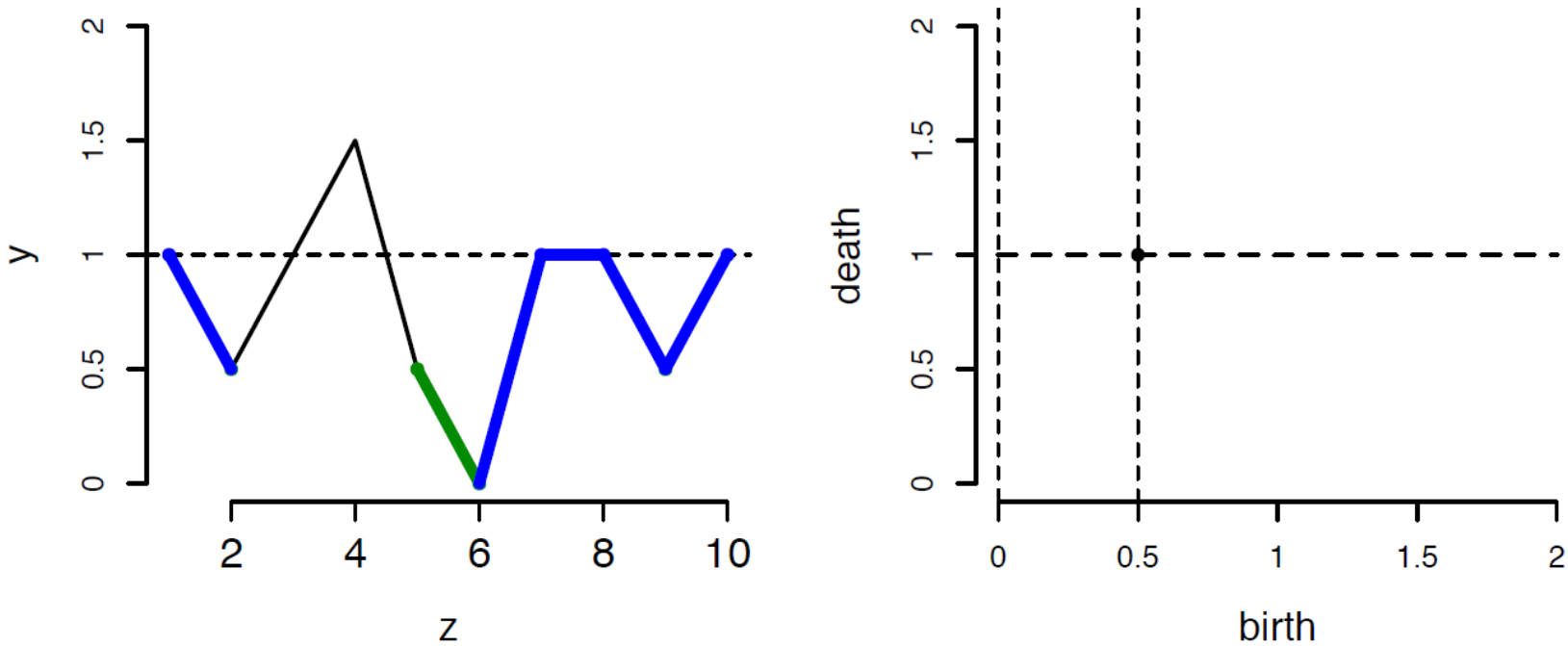

Figure: Figures from Ravishanker and Chen (2019)

Morse Function

- Time series data $\rightarrow$ Morse function

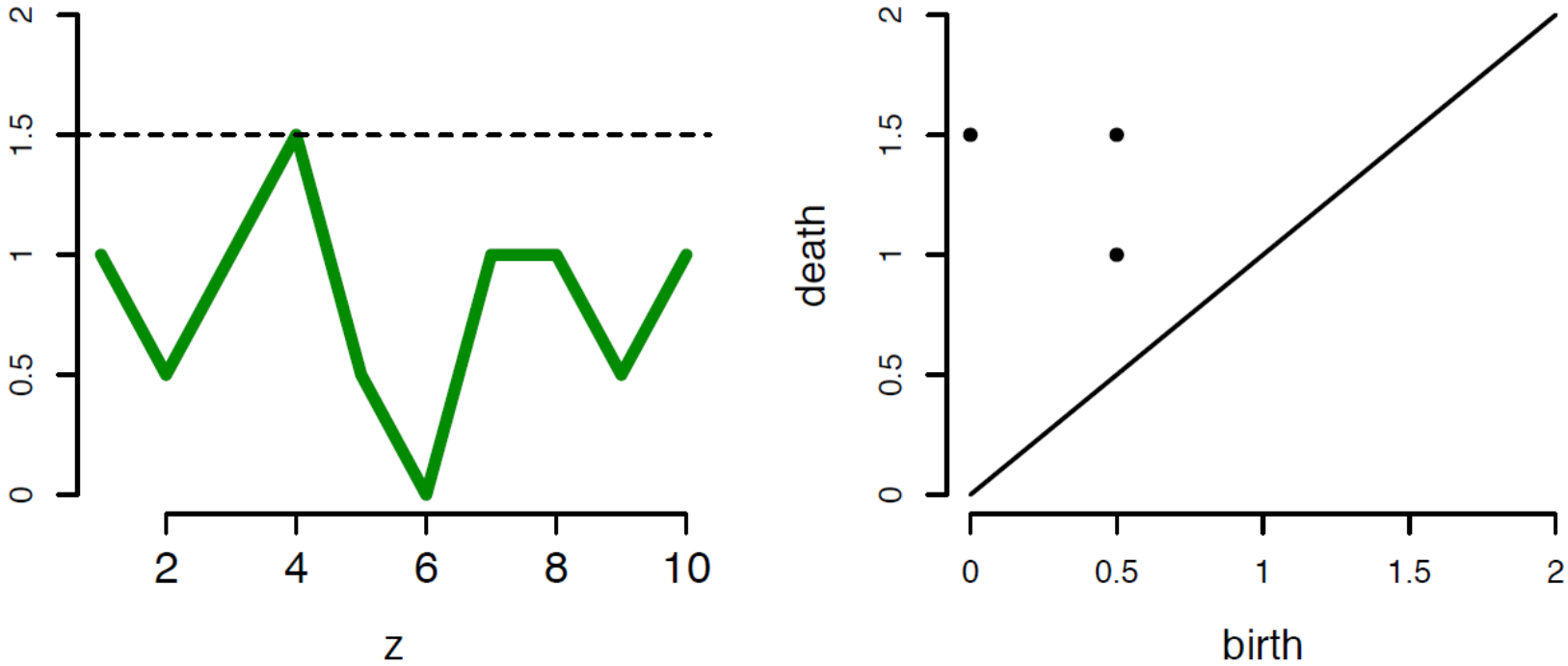

Figure: Figures from Ravishanker and Chen (2019)

Morse Function Example

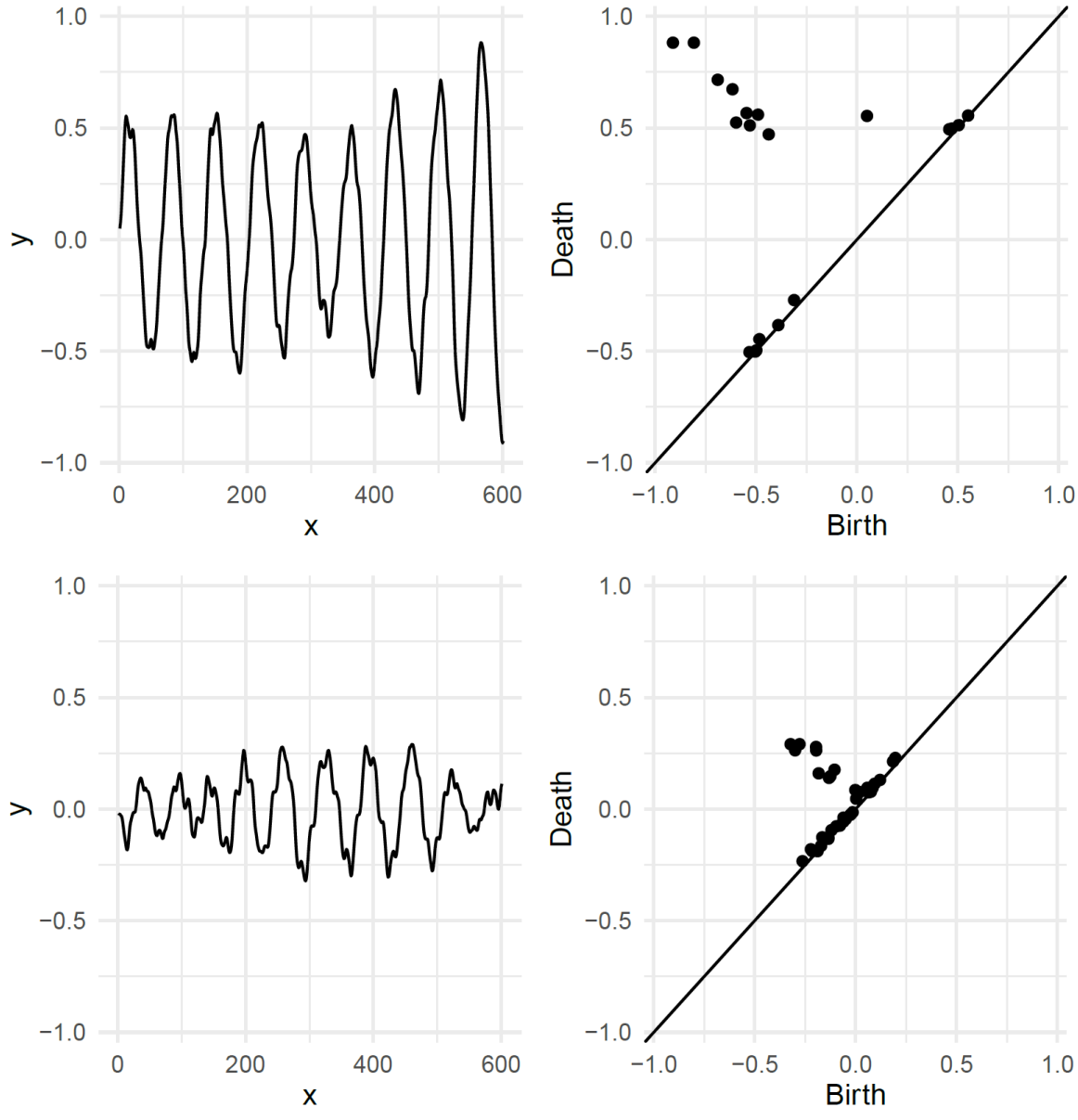

Takens's Delay Embedding

Time series data can be transformed to point clouds by Taken's embedding theorem (Takens, 1981)

- Input: time series
- Parameters: dimension of points d and delay parameter τ
- Time series $\{x_t, t = 1, 2, \ldots, T\}$ is converted to points in d-dimensional space $v_i = (x_i, x_{i+\tau}, \ldots, x_{i+(d-1)\tau})$

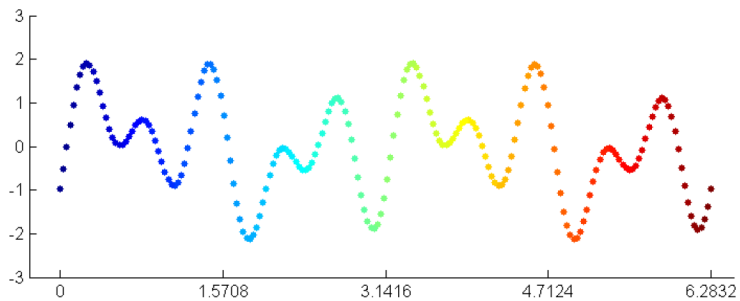

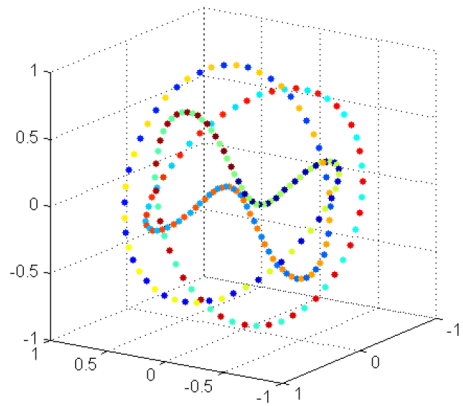

- Topology of point cloud data may reveal the characteristics of time series data such as periodicity
- Compute persistent homology using the transformed point clouds

Takens's Delay Embedding Example

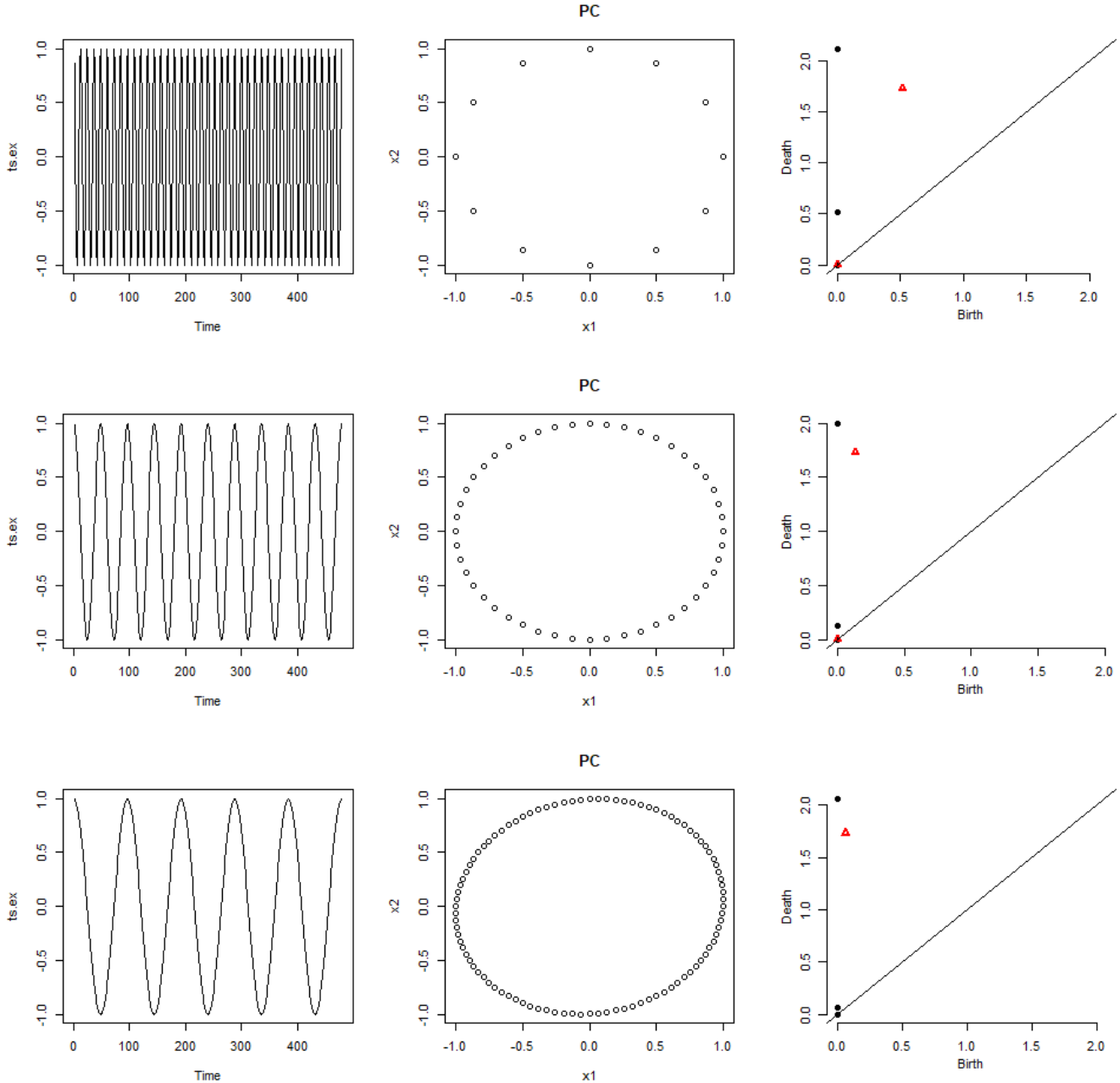

Sliding Windows and 1-Persistence Scoring

- The point cloud embedding has developed to SW1PerS (Sliding Windows and 1-Persistence Scoring) proposed by Perea et al. (2015)
- SW1PerS detects periodicity of noisy time series data and topological features are robust to differences in time series data such as amplitude, phase, and frequency.

References I

Crawford, L., Monod, A., Chen, A. X., Mukherjee, S., and Rabadán, R. (2020), "Predicting clinical outcomes in glioblastoma: an application of topological and functional data analysis," *Journal of the American Statistical Association*, 115, 1139–1150.

Davami, P. (2015), "3D Tomography," *Arya Electron Optic Ltd.*, `http://www.arya-eo.com/3D%20Tomography.htm`.

Galton, F. (1892), *Finger Prints*, McMillan, London.

Moon, C. and Andrew, M. (2019a), "Bentheimer networks," `http://www.digitalrocksportal.org/projects/223`.

— (2019b), "Intergranular Pore Structures in Sandstones," `http://www.digitalrocksportal.org/projects/222`.

Perea, J. A., Deckard, A., Haase, S. B., and Harer, J. (2015), "SW1PerS: Sliding windows and 1-persistence scoring; discovering periodicity in gene expression time series data," *BMC bioinformatics*, 16, 1–12.

Ravishanker, N. and Chen, R. (2019), "Topological data analysis (TDA) for time series," *arXiv preprint arXiv:1909.10604*.

References II

Robins, V., Saadatfar, M., Delgado-Friedrichs, O., and Sheppard, A. P. (2016), "Percolating Length Scales from Topological Persistence Analysis of Micro-CT Images of Porous Materials," *Water Resources Research*, 52, 315–329.

Stelma, D. (2004), "Appraisal Assessment of Geology at Black Rock Damsite," *U.S. Department of the Interior, Bureau of Reclamation, Pacific Northwest Region*.

Takens, F. (1981), "Detecting strange attractors in turbulence," in *Dynamical systems and turbulence, Warwick 1980*, Springer, pp. 366–381.

Talabi, O., AlSayari, S., Iglauer, S., and Blunt, M. J. (2009), "Pore-scale simulation of NMR response," *Journal of Petroleum Science and Engineering*, 67, 168 – 178.

Wang, S., Chen, A., Yang, L., Cai, L., Xie, Y., Fujimoto, J., Gazdar, A., and Xiao, G. (2018), "Comprehensive analysis of lung cancer pathology images to discover tumor shape and boundary features that predict survival outcome," *Scientific Reports*, 8, 10393.

Wang, Z., Bovik, A. C., Sheikh, H. R., and Simoncelli, E. P. (2004), "Image Quality Assessment: From Error Visibility to Structural Similarity," *IEEE transactions on image processing*, 13, 600–612.

References III

Weller, R. (2004), "Photos of Rocks," *Cochise College*.

Xu, X., Cisewski-Kehe, J., Green, S. B., and Nagai, D. (2019), "Finding cosmic voids and filament loops using topological data analysis," *Astronomy and Computing*, 27, 34–52.

Yoon, H. and Dewers, T. A. (2013), "Nanopore Structures, Statistically Representative Elementary Volumes, and Transport Properties of Chalk," *Geophysical Research Letters*, 40, 4294–4298.